Research Paper

GEOSPHERE

GEOSPHERE, v. 17, no. 5

https://doi.org/10.1130/GES02296.1

11 figures; 1 table; 1 set of supplemental files
(1 additional supplemental file hosted by EarthChem)

CORRESPONDENCE: snir.attia@nmt.edu

CITATION: Attia, S., Paterson, S.R., Saleeby, J., and Cao, W., 2021, Detrital zircon provenance and depositional links of Mesozoic Sierra Nevada intra-arc strata: Geosphere, v. 17, no. 5, p. 1422–1453, https://doi.org/10.1130/GES02296.1.

Science Editor: David E. Fastovsky
Associate Editor: Nancy Riggs

Received 2 June 2020
Revision received 18 March 2021
Accepted 24 May 2021

Published online 30 August 2021

Detrital zircon provenance and depositional links of Mesozoic Sierra Nevada intra-arc strata

Snir Attia[1,2], Scott R. Paterson[1], Jason Saleeby[3], and Wenrong Cao[4]

[1]Department of Earth Sciences, University of Southern California, Los Angeles, California 90089, USA
[2]New Mexico Bureau of Geology and Mineral Resources, New Mexico Institute of Mining and Technology, Socorro, California 87801, USA
[3]Division of Geological and Planetary Sciences, California Institute of Technology, Pasadena, California 91125, USA
[4]Department of Geological Sciences and Engineering, University of Nevada, Reno, Nevada 89557, USA

ABSTRACT

A compilation of new and published detrital zircon U-Pb age data from Permo-Triassic to Cretaceous intra-arc strata of the Sierra Nevada (eastern California, USA) reveals consistent sedimentary provenance and depositional trends across the entire Sierra Nevada arc. Detrital zircon age distributions of Sierra Nevada intra-arc strata are dominated by Mesozoic age peaks corresponding to coeval or just preceding arc activity. Many samples display a spread of pre-300 Ma ages that is indistinguishable from the detrital age distributions of pre-Mesozoic prebatholithic framework strata and southwestern Laurentian continental margin deposits. Synthesis of detrital zircon age data with tectonostratigraphic constraints indicates that a marine to subaerial arc was established in Triassic time, giving way to widespread shallow- to deep-marine deposition in latest Triassic to Early Jurassic time that continued until the emergence of the arc surface in the Early Cretaceous. No data presented herein require the existence of Mesozoic exotic terranes and/or outboard arcs that were previously hypothesized to have been accreted to the Sierra Nevada. We conclude that Sierra Nevada intra-arc strata formed within a coherent depositional network that was intimately linked to the southwestern United States Cordilleran margin throughout the span of Mesozoic arc activity.

INTRODUCTION

The Mesozoic Sierra Nevada batholith (Fig. 1) is the magmatic footprint of a Cordilleran arc and associated orogenic belt built through and onto an amalgamated basement of both oceanic and continental margin rocks (Bateman, 1992; Kistler, 1993; Chapman et al., 2012). Permian to Cretaceous plutons and coeval intra-arc strata represent arc activity built into and on top of the Sierra Nevada prebatholithic framework along the southwestern United States Cordilleran margin (Bateman, 1992; Saleeby and Dunne, 2015). Intra-arc sedimentary and volcanic strata are generally tilted by multiple deformational events and metamorphosed to greenschist-amphibolite facies (Tobisch et al., 1977; Sorensen et al., 1998). Due to this tectonic overprint, extensive geochronology and lithostratigraphic observations are required to reconstruct the record of arc surface development that these strata preserve. Detrital zircon U-Pb geochronology reveals the potential sources of intra-arc strata and the evolution of depositional networks across the arc surface.

We present a comprehensive compilation of new and published detrital zircon U-Pb geochronology from Permo-Triassic to Cretaceous intra-arc strata spanning the entire Sierra Nevada (Fig. 2). This compilation of 4906 individual analyses from 80 samples (Table 1) is linked to tectonostratigraphic constraints and other records of arc activity to: (1) better constrain the age and provenance of intra-arc strata and reconstruct Sierra Nevada surface evolution; (2) consider implications for depositional systems, paleogeography, and paleo-tectonics at the arc scale and across the southwestern Cordilleran margin; and (3) unravel the relationship of arc surface processes to episodic arc and orogenic activity. We begin with an overview of the pre-Cenozoic evolution of the Sierra Nevada as well as a summary of previous work on the stratigraphy and detrital zircon geochronology of metamorphic wall-rock pendants. We then present the geochronology and statistical methods used in this study, results of new detrital zircon U-Pb geochronology analyses, and statistical comparison of the compiled data. The detrital zircon provenance of Sierra Nevada intra-arc strata reveals a mix of possible sources for Precambrian–Paleozoic detrital zircon grains across the southwestern Cordillera and is consistent with derivation of Mesozoic detrital ages from coeval to preceding arc activity. In contrast with previous models of a complex Mesozoic history of outboard terrane and/or arc accretion, fragmented sedimentary dispersal networks, and large displacements along intra-batholithic transforms, the consistent provenance and depositional trends demonstrated herein indicate that Sierra Nevada intra-arc strata formed within a coherent depositional system intimately linked to the southwestern Cordilleran margin.

GEOLOGIC BACKGROUND

Arcs and orogens of the southwestern Cordilleran margin initiated during the late Paleozoic to early Mesozoic transition from the western Laurentian passive margin to an active convergent margin (Burchfiel and Davis, 1972). Neoproterozoic–Paleozoic strata with distinct provenance and postdepositional

Snir Attia https://orcid.org/0000-0001-8582-8197

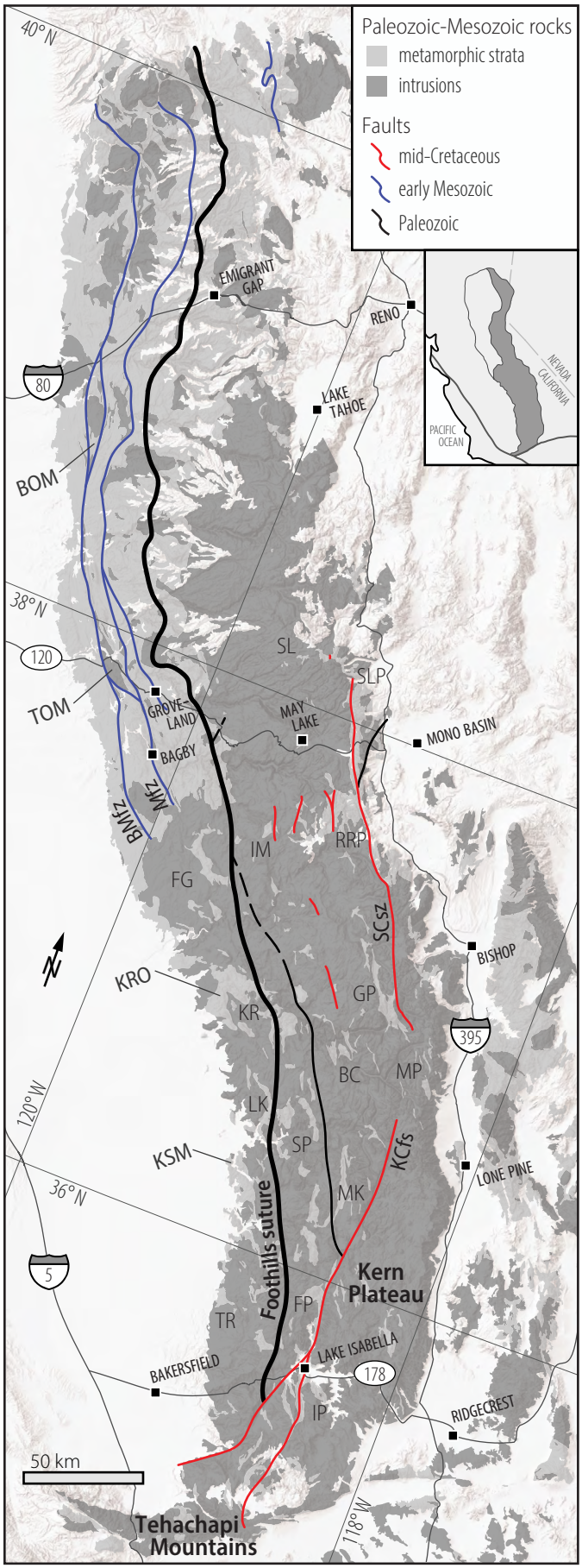

Figure 1. Sierra Nevada geographic reference map with generalized geology adapted from Jennings (2010). Faults: BMfz—Bear Mountains fault zone; KCfs—Kern Canyon fault system; Mfz—Melones fault zone; SCsz—Sierra Crest shear zone. Ophiolite assemblages: BOM—Bear Mountains ophiolitic mélange; KRO—Kings River ophiolite; KSM—Kaweah serpentinite mélange; TOM—Tuolumne ophiolitic mélange. Pendants: BC—Boyden Cave; FG—Fine Gold intrusive suite area; FP—Fairview; GP—Goddard pendant; IM—Iron Mountain; IP—Isabella; LK—Lake Kaweah; KR—Lower Kings River; MK—Mineral King; MP—Mount Pinchot; RRP—Ritter Range; SL—Snow Lake; SLP—Saddlebag Lake; SP—Sequoia Park; TR—Lower Tule River.

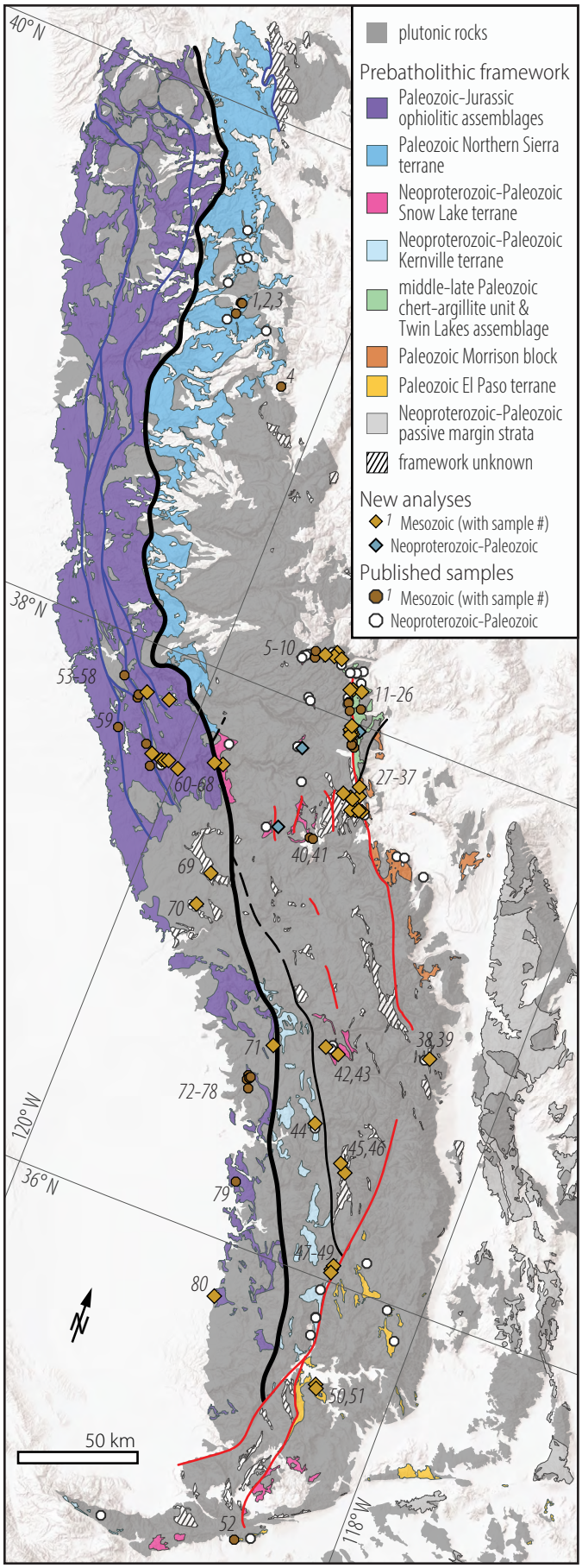

Figure 2. Sample locations overlain onto prebatholithic framework strata of the Sierra Nevada adapted from Attia et al. (2018) and sources therein. Sample information, numbers assigned to samples of Permo-Triassic to Cretaceous strata, and data sources given in Table 1. Map extent and faults same as in Figure 1.

TABLE 1. DETRITAL ZIRCON SAMPLE SUMMARY

Sample name	Sample no.	Location*		MDA# (Ma)	Depositional age	Reference
		Easting	Northing			
Northern Sierra Nevada						
EPF	4	221383	4329726	178	Lower Jurassic	Christe et al., 2018
BVS	1	194387	4357493	187	"	Christe et al., 2018
Sea2000-SCF	2	194455	4357453	200	"	Spurlin et al., 2000
Sea2000-UUT	3	193504	4352591	**255	Triassic	Spurlin et al., 2000
Eastern Sierra Nevada						
DL16-35-a	29	304337	4178781	101	mid-Cretaceous	This study (IESNI000P##)
K-34	17	295074	4212648	117	Lower Cretaceous	Cao et al., 2015
EC345	10	277456	4230560	136	lowermost Cretaceous	This study (IESNI000D)
Mea10a-JT14	7	273090	4231376	144	"	Memeti et al., 2010a
EM16-50-c	31	308783	4177765	148	Middle-Upper Jurassic	This study (IESNI000R)
VT16-2-b	32	312920	4174218	152	"	This study (IESNI000Y)
EC141	8	281240	4231351	154	"	This study (IESNI000E)
EC46	9	284521	4231175	162	"	This study (IESNI000G)
2-68	18	298179	4206033	163	"	This study (IESNI000K)
S-31	21	299075	4203335	171	"	This study (IESNI000N)
VT15-28	33	312886	4174217	***N.D.	"	This study (IESNI000X)
A-158	28	311023	4179913	185	Lower Jurassic	This study (IESNI000U)
S-33	14	293459	4216017	186	"	Cao et al., 2015
S-40	15	293455	4215567	187	"	Cao et al., 2015
3-100	20	298574	4204080	191	"	This study (IESNI000L)
B-49B	30	307872	4178063	193	"	This study (IESNI000Q)
EC544	13	292943	4220577	194	"	This study (IESNI000H)
NR15-98	27	309790	4183553	194	"	This study (IESNI000T)
3-57	19	298608	4205001	**212	Lower Jurassic(?)	This study (IESNI000M)
VT15-9-c	35	312611	4174056	208	uppermost Triassic	This study (IESNI000W)
VT15-15-a	36	311528	4173770	210	"	This study (IESNI000V)
VT15-20	37	309687	4173267	216	"	This study (IESNI000S)
S-1823	39	375610	4085541	216	Triassic	This study (IESNI0010)
TCL-13-5	26	301573	4198736	217	"	Ardill et al., 2020
VT15-3-a	34	314306	4174216	217	"	This study (IESNI000Z)
TP-7	23	300724	4200625	219	"	Ardill et al., 2020
TP-1	24	300967	4199767	220	"	Ardill et al., 2020
KA-9	25	300695	4199512	220	"	Ardill et al., 2020
EC538	12	293373	4220867	**220	"	This study (IESNI000I)
K-57	16	299270	4214813	221	"	Cao et al., 2015
EC472	11	297051	4221271	225	"	This study (IESNI000J)
EC386	6	281847	4233194	230	"	This study (IESNI000F)
S-23	22	299444	4203232	247	"	This study (IESNI000O)
S1822	38	374555	4086173	255	Permo-Triassic	Attia et al., 2018
1-96	-	300913	4205737	***N.D.	mid-Paleozoic	This study (IESNI001D)
Axial Sierra Nevada						
Mea10a-JT013	40	298499	4157381	97	mid-Cretaceous	Memeti et al., 2010
BCP-6	42	334429	4077096	114	Lower Cretaceous	This study (IESNI0001)
Mea10a-JT-09	41	297845	4157323	183	Lower Jurassic	Memeti et al., 2010
Mea10a-SLP-5	5	273761	4228634	188	"	Memeti et al., 2010
09-KK-1	43	338950	4075188	**194	"	This study (IESNI0002)
ML-262-3	-	280789	4190815	N.A.	lower Paleozoic	This study (IESNI001F)
FD-2	-	282575	4156502	N.A.	lower Paleozoic	This study (IESNI001E)

(*continued*)

TABLE 1. DETRITAL ZIRCON SAMPLE SUMMARY (*continued*)

Sample name	Sample no.	Location*		MDA# (Ma)	Depositional age	Reference
		Easting	Northing			
Southern Sierra Nevada						
050611-3	49	368265	3990624	142	lowermost Cretaceous	This study (IESNI0016)
050611-2	47	368098	3990849	159	Jurassic	This study (IESNI0015)
02SS06	50	377986	3942469	171	"	This study (IESNI0018)
14SS03	51	377944	3941470	178	"	This study (IESNI0017)
050611-1	48	368015	3990844	***N.D.	Jurassic(?)	This study (IESNI0014)
MK318	45	356301	4032907	187	Lower Jurassic	This study (IESNI0012)
09-KK-4	44	341569	4043016	**188	"	This study (IESNI0011)
08TC44	52	368106	3870470	238	Triassic	Chapman et al., 2012
MK23	46	359278	4029993	265	"	This study (IESNI0013)
Central Western Metamorphic Belt						
Sal82-MLB1	53	201347	4194460	###198	Upper Jurassic(?)	Saleeby, 1982
PB65A	58	209450	4188200	153	Middle-Upper Jurassic	Snow and Ernst, 2008
PB131A	62	219700	4170600	154	"	Snow and Ernst, 2008
PB04B	57	209700	4188900	157	"	Snow and Ernst, 2008
MR-5	61	252911	4172876	157	"	This study (IESNI000C)
PB158A	59	206200	4173200	159	"	Snow and Ernst, 2008
PB23A	68	224300	4162500	160	"	Snow and Ernst, 2008
MR-6	60	250155	4173165	**160	"	This study (IESNI000B)
MR-7	67	235751	4164695	168	"	This study (IESNI000A)
CH-MR-9	65	229405	4166071	170	"	This study (IESNI0008)
CH-MR-1	64	229887	4166555	171	"	This study (IESNI0009)
MVPriest	56	212021	4190056	172	"	This study (IESNI0003)
SP-2	54	222452	4190584	**467	"	This study (IESNI0005)
SP-3	55	212667	4190486	***N.D.	"	This study (IESNI0004)
Bagby1	63	223414	4167039	206	uppermost Triassic	This study (IESNI0006)
CH-MR-7	66	228019	4165979	255	Permo-Triassic	This study (IESNI0007)
Southern Western Metamorphic Belt						
MM-GP-03	72	307374	4055032	135	lowermost Cretaceous	Martin and Clemens-Knott, 2015
MM-GP-02	73	307329	4054955	135	"	Martin and Clemens-Knott, 2015
MM-GP-07	77	307305	4053154	135	"	Martin and Clemens-Knott, 2015
MM-GP-09	78	309073	4049828	136	"	Martin and Clemens-Knott, 2015
MM-GP-13	76	308144	4054059	138	"	Martin and Clemens-Knott, 2015
MM-GP-12	75	308038	4054155	140	"	Martin and Clemens-Knott, 2015
MM-GP-08	74	307663	4054350	160	"	Martin and Clemens-Knott, 2015
C9	79	317567	4011365	165	Middle-Upper Jurassic	Saleeby, 2011
FG-2-2	70	262385	4114246	165	"	This study (IESNI0019)
09-KK-5	80	325497	3962710	**173	Middle Jurassic(?)	This study (IESNI001C)
VM-30	71	312773	4069702	***N.D.	"	This study (IESNI001B)
SN-11-2	69	263639	4128398	187	Lower Jurassic	This study (IESNI001A)

Note: Dash indicates that sample number was not assigned.
*UTM coordinates given in NAD27 zone 11.
#MDA—Maximum depositional age, determined by center of youngest age peak.
**Poorly constrained MDA.
##SESAR (System for Earth Sample Registration) sample IGSN in parentheses.
***N.D.—no reliable interpreted maximum depositional age.
###MDA based on multigrain fraction analysis.

histories that comprise the Sierra Nevada prebatholithic framework were juxtaposed and emplaced along the truncated southwestern Laurentian margin prior to the Permian–Triassic initiation of Cordilleran arc magmatism (Stone and Stevens, 1988; Dunne and Suczek, 1991; Saleeby and Busby, 1993; Schweickert and Lahren, 1993; Stevens and Greene, 1999; Stevens et al., 2005; Memeti et al., 2010; Saleeby, 2011; Chapman et al., 2012, 2015; Saleeby and Dunne, 2015; Attia et al., 2018; Cecil et al., 2019). Prebatholithic framework strata consist of three broad groups: (1) Neoproterozoic–Paleozoic strata of the Morrison block and Snow Lake terrane that have been displaced relatively little from their original sites of deposition and are thus parautochthonous to the southwestern Laurentian continental margin; (2) lower Paleozoic, deep-marine strata of the Shoo Fly complex, Kernville terrane, and El Paso terrane that show detrital zircon ages indicative of derivation from across western Laurentia and are thus considered allochthonous; and (3) middle to upper Paleozoic shallow-marine deposits of the Northern Sierra terrane and Twin Lakes assemblage that are likely related to fringing arcs developed outboard of the western Laurentian margin (Attia et al., 2018).

Mesozoic magmatism in the central Sierra Nevada (CSN) was highly episodic (Fig. 3A), expressed as three flare-ups of increased magma addition rates centered at ca. 220, 160, and 100 Ma separated by magmatic lulls (Bateman and Wahrhaftig, 1966; Armstrong and Ward, 1993; Paterson and Ducea, 2015; Kirsch et al., 2016; Ardill et al., 2018; Attia et al., 2020). Erupted zircons from metavolcanic rocks across the CSN show dominantly juvenile to intermediate initial Hf isotopic compositions (Fig. 3B), indicating that Sierra Nevada arc flare-ups were characterized by increased juvenile mantle magma input (Attia et al., 2020). The CSN also experienced multiple phases of Mesozoic deformation (Fig. 3C), culminating in a mid-Cretaceous orogenic phase localized in the axial and eastern CSN (Schweickert et al., 1984; Edelman et al., 1989; Paterson et al., 1989; Tobisch et al., 1989, 1995, 2000; Sharp et al., 2000; Cao et al., 2015; Saleeby and Dunne, 2015). Sierra Nevada intra-arc strata exposed in metamorphic wall-rock pendants preserve a fragmented record of Mesozoic surface development in response to arc and orogenic activity (Figs. 2, 3D, and 4).

By mid-Triassic time, the earliest phase of arc magmatism was established along the southwestern Cordilleran margin from Sonora, across the Mojave Desert, to the Sierra Nevada and into western Nevada (Barth et al., 1997, 2011; Proffett and Dilles, 2008; Arvizu and Iriondo, 2015; Cao et al., 2015; Cecil et al., 2019). Lower Mesozoic intra-arc strata of the Sierra Nevada have been proposed to record incipient Late Triassic arc-normal extension that waxed into the Early Jurassic and potentially led to the tectonic emplacement and denudation of the Snow Lake terrane (Busby-Spera 1988; Saleeby and Busby, 1993; Chapman et al., 2015; Saleeby and Dunne, 2015). Deposition continued throughout Middle to Late Jurassic "Nevadan" orogenic activity (Paterson et al., 1987; Tobisch et al., 1989; Saleeby and Dunne, 2015). In latest Jurassic to Early Cretaceous time, arc activity waned, resulting in a magmatic lull coincident with initiation of Great Valley Group forearc deposition and the emergence of the Sierra Nevada arc (Paterson and Ducea, 2015; Orme and Surpless, 2019). The subsequent Early to Late Cretaceous arc flare-up, which was accompanied by a mid-Cretaceous orogenic event, was built across all older units and marked the final stage of Mesozoic arc activity in the Sierra Nevada (Bateman, 1992; Tobisch et al., 1995; Ducea, 2001).

Sierra Nevada Intra-Arc Strata

Sierra Nevada intra-arc strata spanning Permo-Triassic to mid-Cretaceous time (Fig. 4) have generally been grouped into locally defined, informal sequences. Below, we present a summary of Mesozoic tectonostratigraphic relationships and previously published detrital zircon geochronology, including previous interpretations of depositional settings based principally on relict sedimentary textures, lithostratigraphic associations, and limited fossil determinations (Figs. 1, 2, 3D, and 4; Table 1).

Eastern Sierra Nevada

Paleozoic assemblages were tectonically juxtaposed along the southwestern Laurentian margin prior to the development of a regional Middle Permian to mid-Triassic unconformity (Figs. 2 and 4; Attia et al., 2018). These Paleozoic units are overlain by the Triassic Koip sequence, consisting of metavolcanic rocks and interbedded siliciclastic and volcaniclastic strata interpreted as subaerial to submarine deposits (Figs. 1, 3D, and 4; Brook, 1974, 1977; Fiske and Tobisch, 1978; Tobisch et al., 2000; Barth et al., 2012, 2018; Paterson and Memeti, 2014; Cao et al., 2015; Cao, 2016). Published detrital zircon analyses from Upper Triassic Koip sequence strata in the Saddlebag Lake pendant (SLP) show unimodal detrital age distributions with mid-Late Triassic peaks and few older ages (Cao et al., 2015; Ardill et al., 2020). Uppermost Triassic strata in the Ritter Range pendant (RRP), representing the top of the Koip sequence, consist of interbedded volcanic, siliciclastic, carbonate, and calc-silicate layers deposited in shallow-marine environments (Fiske and Tobisch, 1978; Tobisch et al., 2000).

The Koip sequence is unconformably overlain by the informal Sawmill Canyon sequence, which consists of Lower Jurassic to possibly Middle Jurassic shallow-marine siliciclastic sediments, calc-silicate units, volcaniclastic layers, and tuffs (Fig. 4; Greene and Schweickert, 1995; Schweickert and Lahren, 2006; Paterson and Memeti, 2014; Cao et al., 2015). Lower Jurassic SLP strata show detrital zircon age distributions with Early Jurassic major age peaks at ca. 195 Ma, minor Triassic age peaks, and a spread of older mid-Paleozoic, latest Neoproterozoic–Cambrian, and Late Paleoproterozoic ages (Cao et al., 2015). Dominantly volcanic, Middle to Upper Jurassic strata in the RRP are interpreted as submarine deposits given interbedded shales and siltstones, marine fossil occurrences, and extensive slumping (Fig. 4; Fiske and Tobisch, 1978; Tobisch et al., 2000; Barth et al., 2018; Attia et al., 2020). Along with coeval strata in the SLP, we herein refer to this package of Middle to Upper Jurassic strata as the informal Shadow Creek sequence. Finely bedded quartzites and metasiltstones exposed in the Cinko Lake pendant show a unimodal detrital zircon age distribution with

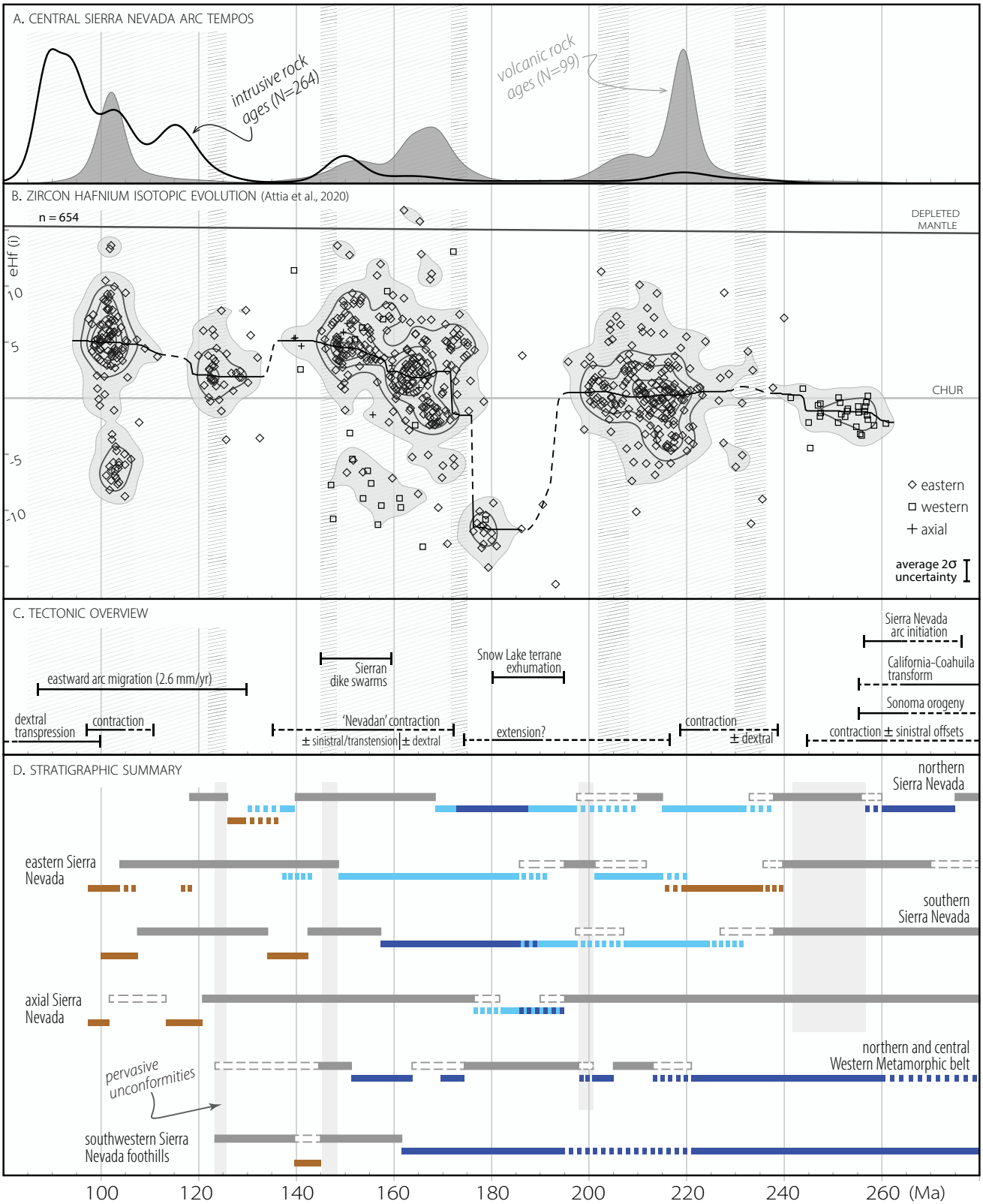

Figure 3. Summary of Sierra Nevada arc tempos, zircon Lu-Hf isotopic evolution of Mesozoic metavolcanic samples, and tectonostratigraphic relationships. (A) Optimized bandwidth kernel density estimates of central Sierra Nevada igneous rock ages, including data from Ardill et al. (2018), Attia et al. (2020), Barth et al. (2018), and data compiled by Kirsch et al. (2016). Compiled geochronology delineates three arc flare-ups, shown as hatched intervals flanked by "shoulders" representing uncertainty in initiation and cessation timing. (B) Zircon initial εHf versus grain age from central Sierra Nevada metavolcanic rocks. Black line representing running median, light gray shaded area representing 95% interval of data density, and medium gray 20% data density contours calculated using HafniumPlotter (Sundell et al., 2019). (C) Sierra Nevada tectonic summary. (D) Stratigraphic overview of Mesozoic Sierra Nevada. Gray bars indicate timing of unconformities, dark blue indicates deep-marine deposition, light blue indicates shallow-marine deposition, and brown indicates terrestrial sedimentation. Dashed bars indicate uncertainty or local variation. See text for discussion and sources. CHUR—CHondritic Uniform Reservoir.

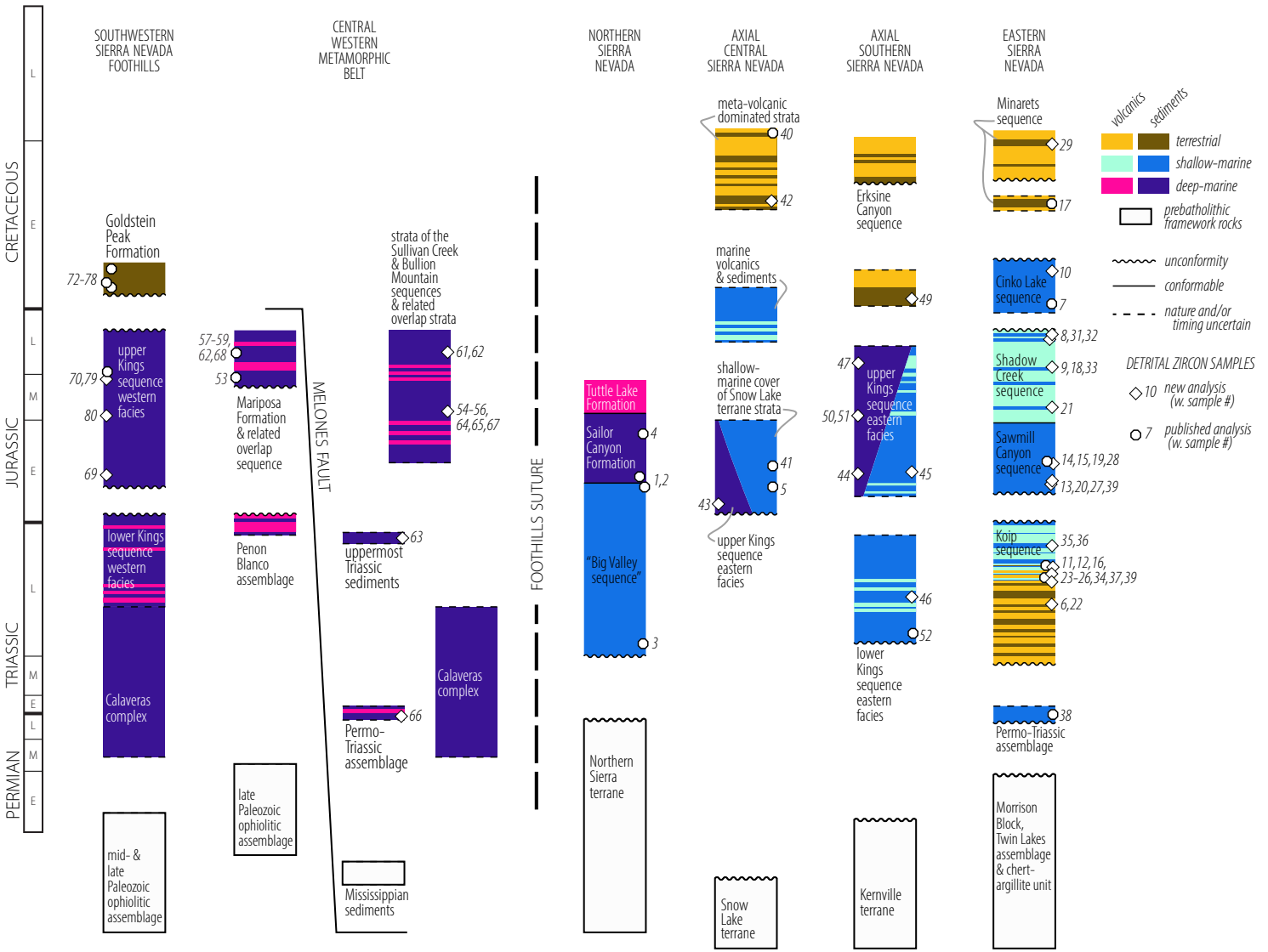

Figure 4. Schematic tectonostratigraphic columns summarizing the stratigraphic relationships, nomenclature, and sample context of key domains of Sierra Nevada intra-arc strata. Sample numbers correspond to those shown in Figure 2 and listed in Table 1.

a major peak at ca. 170 Ma and a subsidiary peak at ca. 144 Ma that provides an earliest Cretaceous maximum depositional age (Memeti et al., 2010).

Triassic through Jurassic rocks of the eastern central Sierra Nevada pendants are overlain by Lower Cretaceous, subaerial, dominantly volcanic strata (Fig. 4; Fiske and Tobisch, 1994; Cao et al., 2015; Ardill et al., 2020; Attia et al., 2020). Fault-bounded slivers of Lower to mid-Cretaceous volcanic strata are variably exposed along the western SLP (Paterson and Memeti, 2014; Cao et al., 2015; Ardill et al., 2020). One published sample of SLP volcanogenic sediments shows a detrital zircon age distribution with a major Jurassic age peak at ca. 165 Ma, a minor age peak at ca. 117 Ma providing a mid-Early Cretaceous maximum depositional age, and a few Paleoproterozoic to Paleozoic ages (Cao et al., 2015).

Farther south along the eastern Sierra Nevada, Permo-Triassic strata exposed in the Mount Pinchot pendant are interpreted to unconformably overlie Neoproterozoic to Cambrian strata (Figs. 1 and 2; Bartley et al., 2001; Attia et al., 2018). One published sample from these strata shows detrital zircon age distribution with a younger spread of Paleozoic ages centered on peaks at ca. 255 and 425 Ma, an older spread of Precambrian ages (Attia et al., 2018). The youngest ages provide a Permo-Triassic maximum depositional age and are interpreted to reflect the early phases of Cordilleran arc magmatism.

Axial Central Sierra Nevada

In pendants along the axial Sierra Nevada, Snow Lake terrane strata are unconformably and structurally overlain by Lower Jurassic, dominantly shallow-marine metasedimentary strata and, locally, Upper Jurassic and Lower to mid-Cretaceous metavolcanic rocks (Figs. 2 and 4; Saleeby et al., 1990; Schweickert and Lahren, 1990; Saleeby and Busby, 1993; Memeti et al., 2010). Lower Jurassic shallow-marine strata in the Snow Lake and Strawberry Mine pendants show multimodal detrital zircon age distributions dominated by pre-Mesozoic ages with Early Jurassic maximum depositional ages (Memeti et al., 2010). In the Strawberry Mine pendant, a volcaniclastic layer within a package of mid-Cretaceous metavolcanic tuffs shows a detrital zircon age distribution dominated by a major age peak at ca. 100 Ma, a minor mid-Jurassic population, and scattered Paleozoic and Mesoproterozoic ages (Memeti et al., 2010).

Southern Sierra Nevada

Dominantly metasedimentary strata of the lower Mesozoic Kings sequence exposed in the Isabella and Fairview pendants are interpreted to record a transition from mid-Triassic to Early Jurassic shallow-marine conditions to Middle to Late Jurassic basinal depositional settings (Fig. 4; Saleeby and Busby, 1993). In the axial southern Sierra Nevada, Kings sequence strata unconformably overlie lower Paleozoic Kernville terrane strata and are structurally juxtaposed with mid-Cretaceous, felsic to intermediate metavolcanic strata (Figs. 2 and 4; Saleeby and Busby-Spera, 1986; Saleeby and Busby 1993; Saleeby, 2011). In the Tylerhorse Canyon pendant of the southernmost Sierra Nevada, schistose metasedimentary rocks show a spread of Mesoproterozoic to Paleoproterozoic ages, a range of Paleozoic ages at ca. 340–400 and 430–470 Ma, and a youngest minor age peak at ca. 238 Ma that provides a mid-Triassic maximum depositional age (Chapman et al., 2012). The Mineral King pendant consists of structurally complex packages spanning Triassic to Cretaceous time that are dominated by metavolcanic strata and include subordinate shallow-marine sediments (Saleeby and Busby, 1993; Klemetti et al., 2014).

Western Metamorphic Belt

The Western Metamorphic belt (WMB) represents the most extensive exposure of metamorphic wall rocks in the Sierra Nevada (Figs. 1 and 2). We herein divide the WMB into three segments: the northern segment extending southwards to 38.5°N, the central segment between 38.5° and 37.5°N, and the southern segment extending southwards from 37.5°N.

Northern WMB. The northern WMB has generally been divided into structurally bounded eastern, central, and western belts. The lowermost Mesozoic strata of the eastern belt, informally referred to as the Big Valley sequence, consist of Upper Triassic to Lower Jurassic deposits that overlie the Paleozoic Northern Sierra terrane (Fig. 4; Harwood, 1988; Christe et al., 2018; Powerman et al., 2020). A basal conglomerate shows a limited number of Middle to Late Permian detrital zircon analyses that provide a maximum depositional age of ca. 255 Ma (Spurlin et al., 2000), whereas a sandstone near the top of this package shows latest Triassic to Early Jurassic detrital zircon ages with a youngest robust cluster at ca. 187 Ma (Christe et al., 2018). These shallow-marine strata are overlain by the deep-marine, Lower to Middle Jurassic Sailor Canyon Formation (Fig. 4; Harwood, 1992). A limited number of detrital zircon grains from a basal sandstone define a single age peak at ca. 200 Ma (Spurlin et al., 2000). A sample from strata correlative with the Sailor Canyon Formation shows a complex detrital age distribution with a Mesozoic major peak at ca. 180 Ma (Christe et al., 2018). Lower to Middle Jurassic strata are overlain by metavolcanic rocks of the Middle to Upper Jurassic Tuttle Lake Formation (Fig. 4; Harwood, 1992). The eastern belt is bounded on the west by the Foothills suture, a key tectonic boundary that separates inboard arc rocks built into Neoproterozoic–Paleozoic continental margin strata from outboard arc rocks associated with mid-Paleozoic to Jurassic ophiolite assemblages (Figs. 1 and 2; Edelman et al., 1989; Saleeby et al., 1989). Successively west of the Foothills suture lie the Paleozoic Feather River belt, Paleozoic to lower Mesozoic (?) basinal deposits potentially correlative to the Calaveras complex, and uppermost Triassic to Upper Jurassic arc rocks and deep-marine strata built into and on top of polygenetic, late Paleozoic to Jurassic ophiolitic complexes (Schweickert et al., 1980; Saleeby, 1982, 1990; Day et al., 1985; Edelman and Sharp, 1989; Saleeby et al., 1989; Day and Bickford, 2004; Smart and Wakabayashi, 2009; Schweickert, 2015).

Central WMB. In the central WMB, the Calaveras–Shoo Fly thrust segment of the Foothills suture separates prebatholithic framework strata to the east from Permian to Jurassic rocks to the west (Figs. 1, 2, and 4; Schweickert et al., 1977; Herzig and Sharp, 1992; Saleeby and Dunne, 2015). The structurally and stratigraphically complex rocks east of the Melones fault have generally been divided into an eastern chert-dominated package, a central argillite-rich package, and a western volcanic greenstone and phyllite package with local chert occurrences (Schweickert et al., 1977, 1988; Bateman et al., 1985; Bhattacharyya, 1986; Herzig and Sharp, 1992). Structural or olistostromal limestone blocks containing Mississippian, Permian, and Triassic fossils that generally young westward are intercalated throughout these packages (Bateman et al., 1985; Herzig and Sharp, 1992). Paterson et al. (1989) interpret these rocks as a structural "mélange" exposing the mid-Paleozoic to Triassic basement underlying the cherts, argillites, and volcanic rocks in the hanging wall of the Melones fault zone with a significant component of deformation predating Melones activity.

West of the Melones fault zone, the latest Triassic–earliest Jurassic Penon Blanco arc assemblage overlies and intrudes late Paleozoic ophiolitic rocks (Figs. 1 and 2; Saleeby, 1982; Bogen, 1985). Penon Blanco arc rocks, along with coeval assemblages in the northern WMB, have been variably interpreted as either (1) a far-traveled arc and/or terrane built over a west-dipping subduction zone that was accreted in Early to Late Jurassic time or (2) as an outboard arc assemblage associated with forearc rifting and/or extension that was built into already accreted basinal rocks over an east-dipping subduction zone (Schweickert et al., 1984; Tobisch et al., 1989; Saleeby, 1990; Dilek et al., 1991; Graymer and Jones, 1994; Snow and Scherer, 2006; Snow, 2007). Triassic–Jurassic rocks are unconformably overlain by Upper Jurassic turbiditic slates, graywackes, and interfingering volcanic and volcaniclastic strata with detrital zircon samples that show mid-Jurassic major age peaks, subsidiary Paleozoic ages, and a spread of Proterozoic ages (Fig. 4; Behrman and Parkison, 1978; Bogen, 1985; Tobisch et al., 1989; Snow and Ernst, 2008).

Southern WMB. Exposures of metamorphic wall rocks in the southwestern Sierra Nevada extend southwards from the central WMB (Fig. 2). Pendants in the vicinity of the Fine Gold intrusive suite (Fig. 1) preserve previously undated sedimentary and volcanic strata that have been variably interpreted as southward continuations of tectonostratigraphic belts of the central WMB (Russell and Cebull, 1977; Schweickert et al., 1977; Bateman et al., 1983; Bateman, 1992; Saleeby and Busby, 1993). Farther south, metamorphic wall rocks west of the Foothills suture are underlain by the polygenetic, middle to late Paleozoic, Kings-Kaweah ophiolite belt (Figs. 1, 2, and 4; Saleeby, 2011). Chaotic chert and argillite with olistostromal Permian limestone blocks, interpreted as correlative to Calaveras complex strata, grade upwards into the western facies of the Kings sequence (Fig. 4; Schweickert et al., 1977; Saleeby, 1979, 1982; Saleeby and Busby, 1993; Saleeby and Dunne, 2015). One published detrital zircon sample from uppermost Kings sequence turbidites shows a multimodal detrital age distribution with a mid-Jurassic major peak, a mid-Triassic minor peak, scattered Paleozoic ages, and a spread of Precambrian ages (Saleeby, 2011). Lowermost Cretaceous, terrestrial metasedimentary strata of the Goldstein Peak Formation are exposed in the Lake Kaweah pendant (Figs. 1 and 4; Martin and Clemens-Knott, 2015).

METHODS

Geochronology

U-Pb geochronology analyses of zircons from 48 samples of Permo-Triassic to Cretaceous strata and three samples of lower to mid-Paleozoic strata were conducted by laser ablation–inductively coupled–plasma mass spectrometry at the Arizona LaserChron Center (Fig. 1; Table 1; Gehrels et al., 2008). Detailed methods are presented in File S1 in the Supplemental Material[1]). Analyzed zircon grains with a U/Th ratio above 10 were filtered out prior to plotting and statistical comparison to exclude a small number of potentially metamorphic zircon grains. Analyses with U concentrations greater than 1000 ppm were excluded to avoid potential isotopic disturbances. Analyses older than 500 Ma with greater than 20% discordance or 10% reverse discordance were filtered out to exclude effects of Pb-loss or other disturbances of isotopic ratios. Analyses younger than 500 Ma were filtered based on relationships in concordia diagrams generated with Isoplot 3.75 (Ludwig, 2012), excluding those analyses with concordance error ellipses that do not intersect the concordia curve as possibly affected by isotopic ratio disturbances. Maximum depositional ages correspond to the center of the youngest peak composed of at least three grain ages for each sample distribution. Zircon U/Pb isotopic data for all new analyses are presented in Table S2[2]. Detrital zircon analyses of three new samples from lower to mid-Paleozoic strata are included in this study for future reference but are not discussed further herein.

Compilation

We compiled previously published detrital zircon U-Pb ages across the entire Sierra Nevada (Table 1). One multigrain fraction sample analysis (number 53) from the central WMB is included herein as a maximum depositional age constraint, but it does not include corresponding compiled grain analyses (Saleeby, 1982). Prior to data filtering, our compilation contains 4906 grain analyses from 79 samples of Permo-Triassic to Cretaceous strata across the Sierra Nevada with U/Th values compiled for all but three of the samples. These data were generated by multiple researchers using multiple methods at multiple facilities. Methodological choices such as discordance cut-off, filtering of high U/Th analyses, and exclusion of grain ages younger than known depositional ages vary by study, depend on the particular data set, and are somewhat subjective (Gehrels, 2014). Uniform U concentration and U/Th filters have been applied to the entire data set as well as a discordance cut-off for ages greater than 500 Ma using the same criteria as described above, but we have not filtered previously published analyses younger than 500 Ma by concordia diagram relationships.

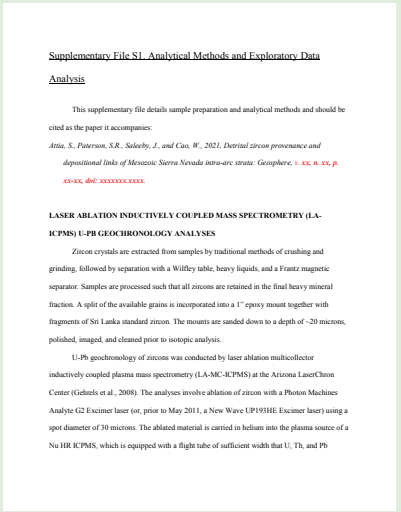

Supplementary File S1. Analytical Methods and Exploratory Data Analysis

This supplementary file details sample preparation and analytical methods and should be cited as the paper it accompanies:

Attia, S., Paterson, S.R., Saleeby, J., and Cao, W., 2021, Detrital zircon provenance and depositional links of Mesozoic Sierra Nevada intra-arc strata: Geosphere, v. xx, n. xx, p. xx–xx, doi: xxxxxxx.xxxx.

LASER ABLATION INDUCTIVELY COUPLED MASS SPECTROMETRY (LA-ICPMS) U-PB GEOCHRONOLOGY ANALYSES

Zircon crystals are extracted from samples by traditional methods of crushing and grinding, followed by separation with a Wilfley table, heavy liquids, and a Frantz magnetic separator. Samples are processed such that all zircons are retained in the final heavy mineral fraction. A split of the available grains is incorporated into a 1" epoxy mount together with fragments of Sri Lanka standard zircon. The mounts are sanded down to a depth of ~20 microns, polished, imaged, and cleaned prior to isotopic analysis.

U-Pb geochronology of zircons was conducted by laser ablation multicollector inductively coupled plasma mass spectrometry (LA-MC-ICPMS) at the Arizona LaserChron Center (Gehrels et al., 2008). The analyses involve ablation of zircon with a Photon Machines Analyte G2 Excimer laser (or, prior to May 2011, a New Wave UP193HE Excimer laser) using a spot diameter of 30 microns. The ablated material is carried in helium into the plasma source of a Nu HR ICPMS, which is equipped with a flight tube of sufficient width that U, Th, and Pb

[1]Supplemental Material. File S1: Detrital zircon U-Pb geochronology analytical methods and details of exploratory data analysis. File S3: Detrital zircon age compilation from pre-Cenozoic strata across the Sierra Nevada (with two tables). Please visit https://doi.org/10.1130/GEOS.S.14673861 to access the supplemental material, and contact editing@geosociety.org with any questions.

[2]Table S2. Complete data table, which contains isotopic ratios, dates, and uncertainties, is available through the EarthChem library, https://doi.org/10.26022/IEDA/111682.

Sample information is given in Table 1, multidimensional scaling exploratory data analysis results are given in File S1, and compiled detrital zircon age data are given in File S3 in the Supplemental Material (footnote 1).

RESULTS

Detrital Zircon U-Pb Geochronology

Eastern Central Sierra Nevada Pendants (Fig. 5A)

Detrital zircon U-Pb ages were analyzed for 23 samples from Mesozoic strata of the Saddlebag Lake (SLP) and Ritter Range (RRP) pendants in the eastern CSN (Figs. 1, 2, and 4). Eight samples from Upper Triassic shales to sandstones of the Koip sequence from both the RRP and SLP show similar detrital age distributions and have been plotted together. These Triassic samples show very few detrital ages older than 300 Ma and dominantly unimodal Triassic age peaks that are slightly older or approximately equal to strata depositional ages where known. Lower Jurassic samples of the Sawmill Canyon sequence from the RRP and SLP form two groups of distinct detrital age distributions. Three SLP samples from quartzites intercalated with subordinate calc-silicate layers are dominated by pre-Mesozoic ages with limited Early Jurassic to Late Triassic ages between ca. 185–215 Ma. The composite distribution shows a spread of ages between ca. 300–500 Ma with minor peaks at ca. 410 and 480 Ma, a spread between ca. 900–1400 Ma with a peak at ca. 1160 Ma, and a subordinate spread between ca. 1600–2000 Ma. Three RRP samples from coarse-grained sediments are dominated by Early Jurassic to latest Triassic detrital ages with a major age peak at ca. 195 Ma and a subsidiary peak between ca. 205–220 Ma.

Samples from Middle to Upper Jurassic strata of the Shadow Creek sequence in the RRP and SLP generally show dominant mid-Jurassic age peaks and a spread of pre-Mesozoic ages. Three samples from phyllitic siltstones and one sample from a conglomeratic quartzite show similar detrital age distributions with maximum depositional ages from ca. 150–170 Ma. The composite distribution shows Mesozoic age peaks at ca. 150, 170, and 210 Ma. Pre-Mesozoic ages define a major peak at ca. 2500–2600 Ma, minor peak at ca. 1500 Ma, spread of ages between ca. 1000–1200 Ma, and few mid-Paleozoic and latest Neoproterozoic ages. Two samples of siliciclastic sediments (numbers 9 and 18) show unimodal distributions dominated by Jurassic age peaks but have been grouped with the above composite distribution. One sample (number 33) includes no analyses that passed applied filtering criteria and is excluded from Figure 5 and further discussion.

Sample number 10 from interbedded siltstones and sandstones in the Piute Meadows area of the northernmost SLP contains only eight filtered detrital ages that define a unimodal peak at ca. 136 Ma, providing an Early Cretaceous maximum depositional age, and a single Jurassic analysis. One filtered analysis at ca. 90 Ma is significantly younger than independent age constraints and is thus excluded. Sample number 29 from a recrystallized, silty sandstone layer in the Davis Lakes area of the RRP shows a unimodal detrital age distribution with a peak at ca. 101 Ma, providing a mid-Cretaceous maximum depositional age.

Mount Pinchot Pendant (Fig. 5B)

A sample from a conglomerate within a metasedimentary package associated with the Mount Pinchot pendant (Figs. 1 and 2) shows a major detrital age peak at ca. 216 Ma that defines the youngest robust age cluster and provides a mid-Upper Triassic maximum depositional age. Pre-Mesozoic ages form a minor peak at ca. 1400 Ma and a spread between ca. 1600–1850 Ma.

Boyden Cave Pendant (Fig. 5C)

Two samples were collected from Mesozoic strata of the Boyden Cave pendant (Figs. 1 and 2). Sample number 43, collected from the upper turbidite unit of the Boyden Cave pendant that bears Early Jurassic ammonites and bivalves (Saleeby and Busby, 1993), is dominated by pre-Mesozoic detrital ages with major peaks at ca. 420, 600, and 1050 Ma, a minor peak at ca. 1500 Ma, a spread of ages between ca. 1100–1450 Ma, and scattered Paleoproterozoic ages. Sample number 42, collected from a quartzite within mixed schists and gneiss exposed in the westernmost Boyden Cave pendant, shows a unimodal Early Cretaceous age peak that provides a ca. 114 Ma maximum depositional age with a spread of slightly older ages stretching to ca. 130 Ma.

Sequoia Park Pendants (Fig. 5D)

One sample from the Sequoia Park pendants (Figs. 1 and 2) was collected from impure layered quartzite interpreted as a turbidite above a transposed, apparent unconformity above Paleozoic Kernville terrane strata (Saleeby and Dunne, 2015; Attia et al., 2018). This sample (number 44) shows a detrital age distribution with a spread of early Mesozoic, Paleozoic, and Proterozoic ages. The youngest coherent group of detrital ages forms a major peak at ca. 188 Ma, providing an Early Jurassic maximum depositional age. Older ages show major peaks at ca. 385 and 1325 Ma, minor peaks at ca. 1000–1100 and 1625 Ma, and other scattered Proterozoic ages stretching back to ca. 2100 Ma.

Mineral King Pendant (Fig. 5E)

Two samples were collected from Mesozoic strata of the Mineral King pendant (Figs. 1 and 2). Sample number 46 was collected from a medium- to coarse-grained sandstone layer within a package of bedded metasandstones

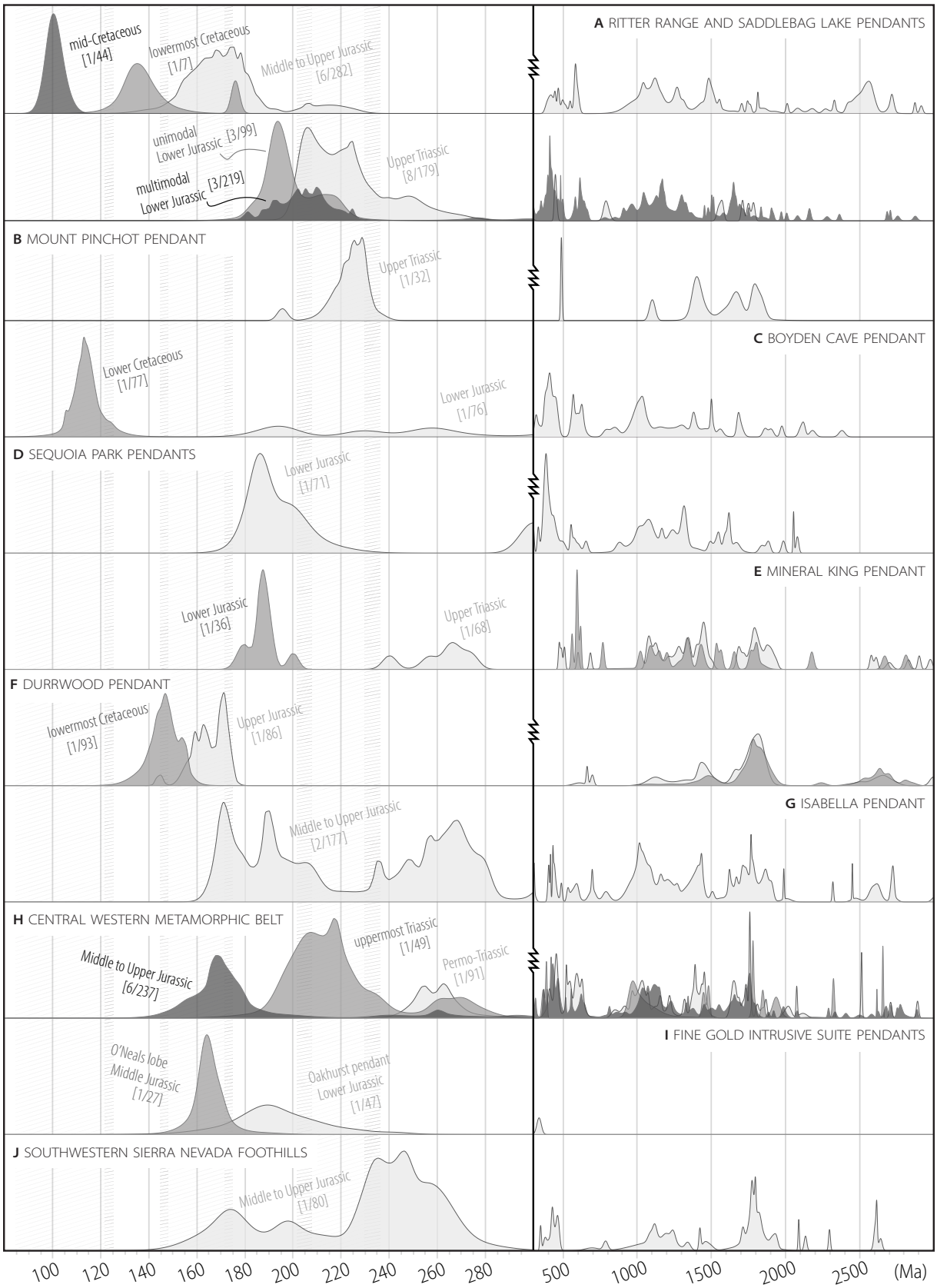

Figure 5. Probability density plots of new detrital zircon age data from Sierra Nevada intra-arc strata grouped by sample location and depositional age. Grayscale fill simply differentiates between different curves. First number in brackets denotes number of sample populations combined to form each distribution; second number indicates total number of zircon ages plotted. Unimodal detrital age distributions are dominated by single age peaks and show few (<10%) pre-300 Ma ages, whereas multimodal distributions show a significant pre-300 Ma detrital age component. Hatched intervals indicate arc flare-up timing. See Table 1 and Table S1 (see text footnote 1) for sample information and complete analytical data.

(Klemetti et al., 2014). This sample shows only a few Mesozoic grains with a spread of older ages that define major peaks at ca. 265, 1450, and 1790 Ma and minor peaks at 1050–1150, 1350, 1680, and 1875 Ma. This sample is assigned a Middle Permian maximum depositional age but is likely part of the Upper Triassic section of the Mineral King pendant (Busby-Spera and Saleeby, 1987). Sample number 45, collected from a volcanogenic sandstone within a structurally complex package of felsic metavolcanic strata, shows a spread of Precambrian detrital ages and a major age peak at ca. 187 Ma that provides an Early Jurassic maximum depositional age.

Durrwood Pendant (Fig. 5F)

Three samples were collected from Mesozoic strata exposed in the Durrwood pendant, located just north of the Fairview pendant (Figs. 1 and 2). Sample number 47 from a meta-siltstone within a package of turbidites is dominated by mid-Jurassic detrital ages that form a major peak at ca. 170 Ma and a subsidiary peak at ca. 160 Ma, providing a Late Jurassic maximum depositional age. Pre-Mesozoic ages define minor peaks at ca. 1450, 1750–1850, and 2670 Ma. Sample number 49, collected from a fine-grained meta-siltstone, is dominated by a major age peak at ca. 145 Ma, providing a Jurassic–Cretaceous maximum depositional age. Precambrian ages define a major age peak ca. 1700 Ma with minor peaks at ca. 1450 and 2650 Ma. Sample number 48 yielded only two analyses that passed the above filters and is excluded from Figure 5 and further discussion.

Isabella Pendant (Fig. 5G)

Two samples (Figs. 1 and 2) were collected from pelitic to psammitic schists that form the upper turbidite unit Isabella pendant of Saleeby and Busby (1993). Both samples show similar distributions with mid-Jurassic maximum depositional ages and major age peaks at ca. 170, 190, and 270 Ma and a spread of early Paleozoic to latest Neoproterozoic ages. Older age define major peaks at ca. 1000–1100, 1430, and 1770 Ma with minor peaks at ca. 1200, 1860, and 2620 Ma.

Central Western Metamorphic Belt (Fig. 5H)

Ten samples from central WMB strata were analyzed for detrital zircon ages. All new samples were collected from east of the Melones fault zone (Figs. 1, 2, and 4). Sample number 66, collected from along the Merced River within a package of structurally complex epiclastic sediments exposed near Sherlock Creek, shows a latest Permian major age peak at ca. 260 Ma and a spread of older Paleozoic to Proterozoic detrital ages with peaks at ca. 450, 520–640, 1050, 1375–1475, 1650, 1770, and 1850 Ma. The youngest robust age cluster gives a maximum depositional age at ca. 255 Ma, and we tentatively assign this sample a Permo-Triassic depositional age. Sample number 63, collected from silty phyllites exposed near the Bagby Campground along the Merced River at the base of the Melones fault hanging wall, shows a major age peak at ca. 215 Ma, a minor peak at ca. 265 Ma, and a subsidiary spread of older Neoproterozoic–Late Mesoproterozoic and mid-Paleoproterozoic ages. The youngest robust age cluster at ca. 206 Ma provides a latest Triassic maximum depositional age.

Five samples collected from siltstones interbedded within packages variably consisting of epiclastic sediments, argillites, cherts, minor carbonates, and volcanic strata along the Merced River east of the Melones fault zone show Middle to Late Jurassic maximum depositional ages spanning ca. 157–171 Ma and similar detrital zircon age distributions. Two of these samples (numbers 60 and 61) were collected from exposures near the Calaveras–Shoo Fly thrust and represent potentially in-folded and/or faulted Jurassic strata within the Calaveras complex. The composite distribution of Middle to Upper Jurassic strata, as well as the individual sample populations, shows a major mid-Jurassic component with a peak at ca. 170 Ma, a subsidiary Early Jurassic population, and very few Triassic ages. Older ages show major peaks at ca. 425, 1025–1175, and 1750 Ma, minor peaks at ca. 625, 1325, and 1650 Ma, and a spread of ca. 800–950 and 1400–1550 Ma ages with scattered analyses stretching back to Archean ages. Only seven filtered analyses from a sixth sample (number 56), collected from an argillite unit west of Groveland, define a unimodal age peak at ca. 170 Ma and are included within the above composite distribution due to the limited number of analyses.

Sample number 55, collected along Highway 120 east of Priest, shows only two analyses that passed the above filters, but both ages are significantly younger than independent constraints, and this sample is given an estimated mid-Jurassic depositional age based on field relationships. Sample number 54, also collected along Highway 120, shows a single ca. 480 Ma analysis that passed filtering criteria and three other coeval, concordant analyses with U concentrations just above the filter threshold. Although these analyses provide a ca. 467 Ma maximum depositional age, the sampled strata are likely as young as mid-Jurassic. Given the limited data, these two samples are excluded from Figure 5 and further discussion.

Fine Gold Intrusive Suite Pendants (Fig. 5I)

Sample number 69 was collected from a siltstone within a sequence of interbedded meta-volcanic and sedimentary strata in the Oakhurst pendant (Figs. 1 and 2). These strata have been previously interpreted as an along-strike continuation of similar rocks east of the Melones fault zone in the central WMB (Bateman, 1992). This sample shows a unimodal distribution with a peak at ca. 190 Ma, several scattered Triassic ages, and one late Paleozoic age. The main age peak provides an Early Jurassic maximum depositional age. Sample number 70 was collected from a siltstone from the O'Neals lobe of the Mountain View

Peak pendant and shows a unimodal detrital age distribution with a peak at ca. 165 Ma, thus providing a Middle to Late Jurassic maximum depositional age.

Southwestern Sierra Nevada (Fig. 5J)

Sample number 80 was collected from a quartzofeldspathic sandstone folded into ophiolitic mélange south of the Tule River (Figs. 1 and 2) and shows a major peak at ca. 245 Ma, a minor peak at ca. 200 Ma, and a youngest robust detrital age cluster that provides a maximum depositional age of ca. 173 Ma. A spread of Paleozoic ages defines a minor peak at ca. 450 Ma. Precambrian ages show a major peak at ca. 1800 Ma and minor peaks at ca. 1120, 1220, and 2620 Ma. Sample number 71, collected from exposures along the Lower Kings River west of the proposed trace of the Foothills suture (Figs. 1 and 2; Saleeby and Busby, 1993; Saleeby and Dunne, 2015), shows only three analyzed zircons that passed the filtering criteria. The limited data preclude a maximum depositional age estimate. This sample is excluded from Figure 5 and further discussion.

Data Compilation

Detrital zircon age data, from 74 of the 80 compiled samples of Sierra Nevada Permo-Triassic to Cretaceous strata, are presented in Figure 6 as composite distributions with samples grouped by depositional age and separated between unimodal and multimodal distributions. Detrital zircon age distributions of Sierra Nevada intra-arc strata can be broken down into three general components: (1) a youngest peak with detrital ages coeval with or just older than strata depositional ages; (2) a subsidiary shoulder of the youngest age peak or separate population with detrital ages corresponding to older phases of arc magmatism; and (3) a complex, multimodal spread of ages older than 300 Ma making up ~1%–90% of distributions (Fig. 6).

The composite distribution of all compiled Permian to Cretaceous detrital ages shows major age peaks at ca. 165 and 225 Ma, minor peaks at ca. 100, 125, 195, and 205 Ma, and a subsidiary spread of 240–270 Ma ages. This composite 80–300 Ma distribution is not representative of the Permian to Cretaceous detrital zircon ages of any single sample of Sierra Nevada intra-arc sediments, none of which show a continuous spread of Mesozoic ages (Fig. 6). Due to sampling bias with respect to geography and stratigraphic time, the relative proportions of peaks in the 80–300 Ma composite age distribution are also not representative of the relative magnitudes of arc magmatism through time (Paterson and Ducea, 2015). The composite distribution of pre-300 Ma ages shows major peaks at ca. 425, 600, 1050, 1150, 1450, 1650, 1700, 1775, and 1825 Ma, minor peaks at 375, 460, 550, 1225, 1320, 1400, 1500, 1900, 1980, 2080, 2575, 2625, and 2700 Ma, with a subsidiary spread of Carboniferous, mid-Neoproterozoic, and early Paleoproterozoic to late Archean ages (Fig. 6). This spread of older ages and, to a lesser extent, the relative proportions of detrital age peaks are representative of this older component in all multimodal facies samples.

Zircon U/Th Values

Figures 7 and 8 present U/Th values of filtered detrital age analyses from intra-arc strata in comparison to several reference records. Zircon U/Th values depend on both parental magma compositions and co-crystallizing phases, which are in turn controlled by the mineral assemblages that are thermodynamically stable at magma source regions and throughout transcrustal magma systems (Davidson et al., 2013; Kirkland et al., 2015). U/Th values of compiled Sierra Nevada detrital zircon analyses are compared to several other zircon age data sets. Zircon U/Th values in arc magmatic systems are generally nonunique, and these comparisons are simply used to assess whether potential provenance interpretations are permissible given the trace-element compositions of analyzed detrital zircons.

Pre–300 Ma analyses are compared to data from Paleozoic to Precambrian prebatholithic framework strata of the Sierra Nevada and to inherited zircons in CSN Mesozoic metavolcanic rocks (Fig. 7; Attia et al., 2018, 2020). U/Th values of these older zircons span similar ranges in Triassic, Jurassic, and Cretaceous samples and broadly overlap with zircon U/Th values of detrital zircons from prebatholithic framework strata and inherited zircons in Mesozoic metavolcanic rocks of the CSN, showing no notable trends or difference between eastern and western Sierra Nevada samples. U/Th values of 80–300 Ma detrital zircons are compared to bedrock zircons from CSN Mesozoic metavolcanic rocks and detrital zircons from intra- and retro-arc strata of the Mojave Desert as well as Great Valley Group fore-arc basin strata (Fig. 8; Barth et al., 2004; Riggs et al., 2013, Stone et al., 2013; Paterson et al., 2017; Surpless et al., 2019; Attia et al., 2020). In Sierra Nevada intra-arc strata, Late Triassic detrital zircon U/Th values range from ~1.0–6.0, Early Jurassic detrital zircons show U/Th values of ~0.6–4.0, Middle to Late Jurassic detrital zircons show U/Th values of ~0.5–6.0, Early Cretaceous detrital zircons show U/Th values of ~1.0–5.5, and mid-Cretaceous grains show U/Th values of ~0.7–3.5 (Fig. 8). No trends or differences are apparent with respect to sample location or geographic affinity.

DISCUSSION

Detrital Zircon Age Components

Below, discussion of pre–300 Ma and 80–300 Ma detrital zircon age components found in Permo-Triassic to Cretaceous strata of the Sierra Nevada is followed by consideration of the provenance of intra-arc strata themselves.

Precambrian–Paleozoic Detrital Ages

Samples with multimodal detrital age distributions that include Precambrian to Paleozoic detrital zircons all show highly similar pre–300 Ma detrital age populations (Fig. 6), and we thus consider the provenance of this older

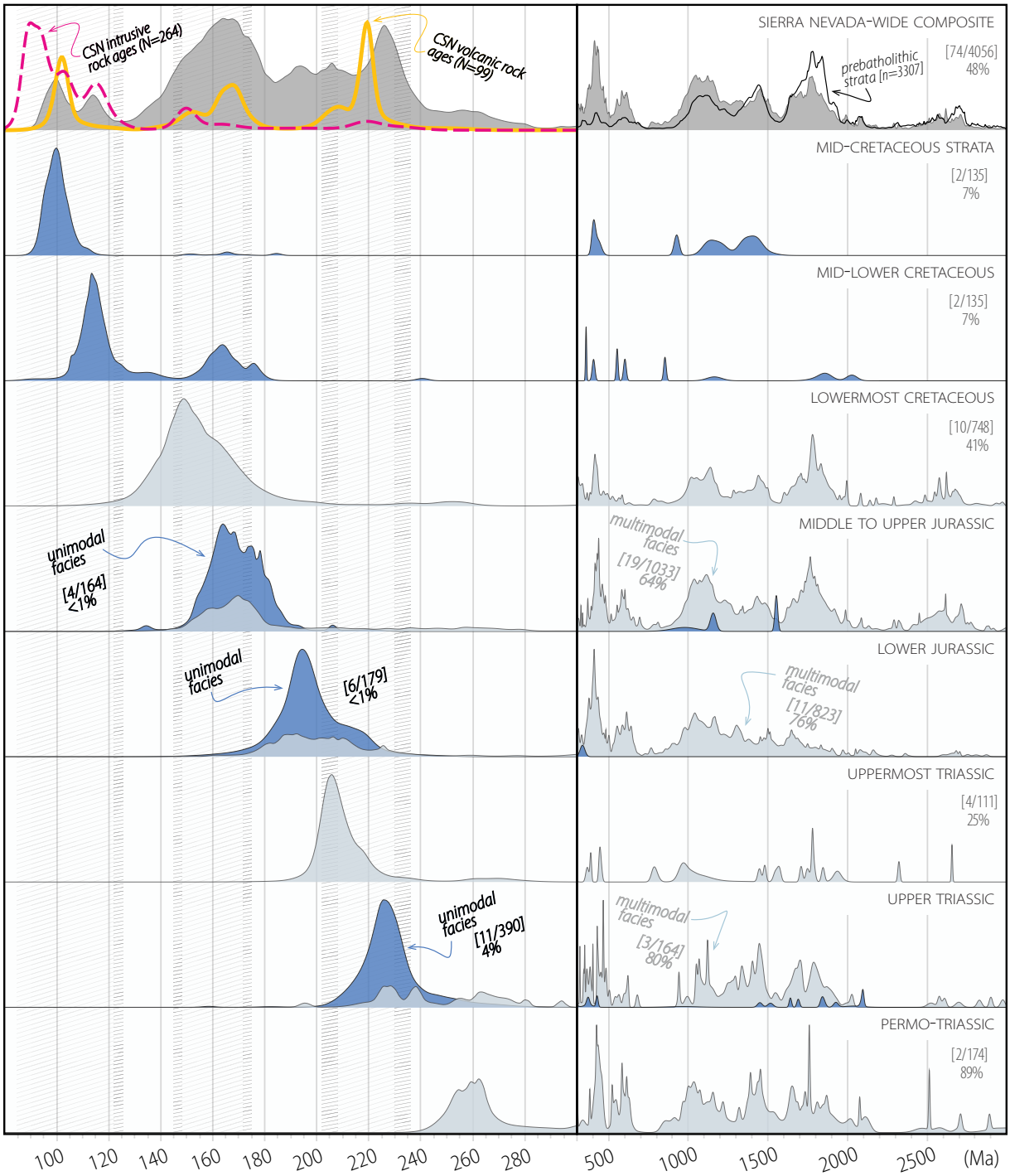

Figure 6. Summary of all Sierra Nevada intra-arc strata detrital zircon ages as composite probability density plots grouped by depositional age and distribution characteristics. First number in brackets denotes number of sample populations combined to form each distribution; second number indicates total number of zircon ages plotted; percentage indicates proportion of ages older than 300 Ma for each composite distribution. Hatched intervals indicate arc flare-up timing. Igneous rock age reference curves same as in Figure 3A; composite distribution of prebatholithic framework strata is taken from compilation of Attia et al. (2018). CSN—central Sierra Nevada.

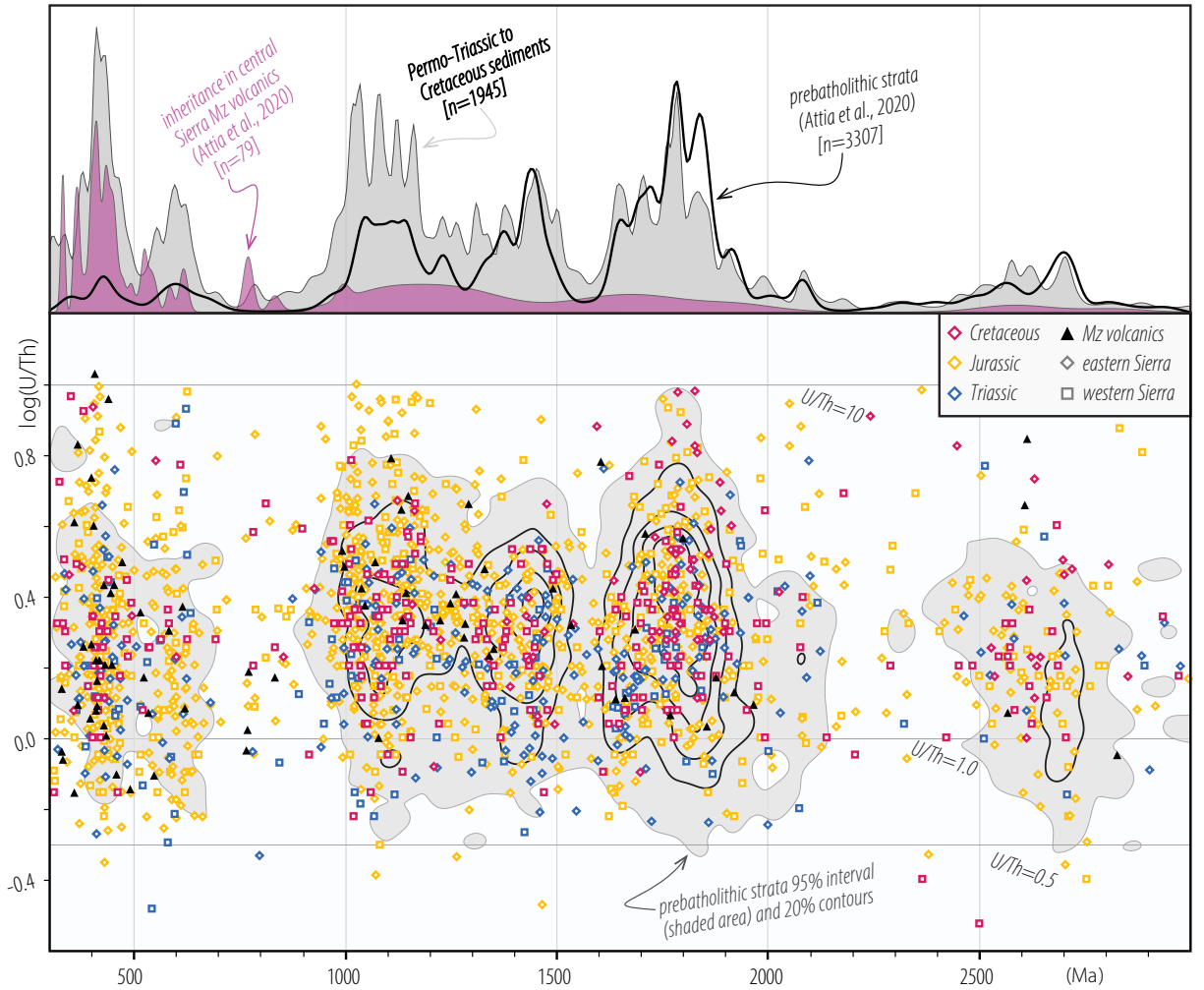

Figure 7. Comparison of pre-300 Ma detrital zircon ages and U/Th values in Sierra Nevada Mesozoic intra-arc strata to prebatholithic framework strata and inherited zircons in Mesozoic central Sierra Nevada volcanic samples. Both ages and U/Th values show broad overlap with no distinct subpopulations. Zircon ages shown as probability density plots of composite distributions. Data contours plotted in HafniumPlotter (Sundell et al., 2019). Mz—Mesozoic.

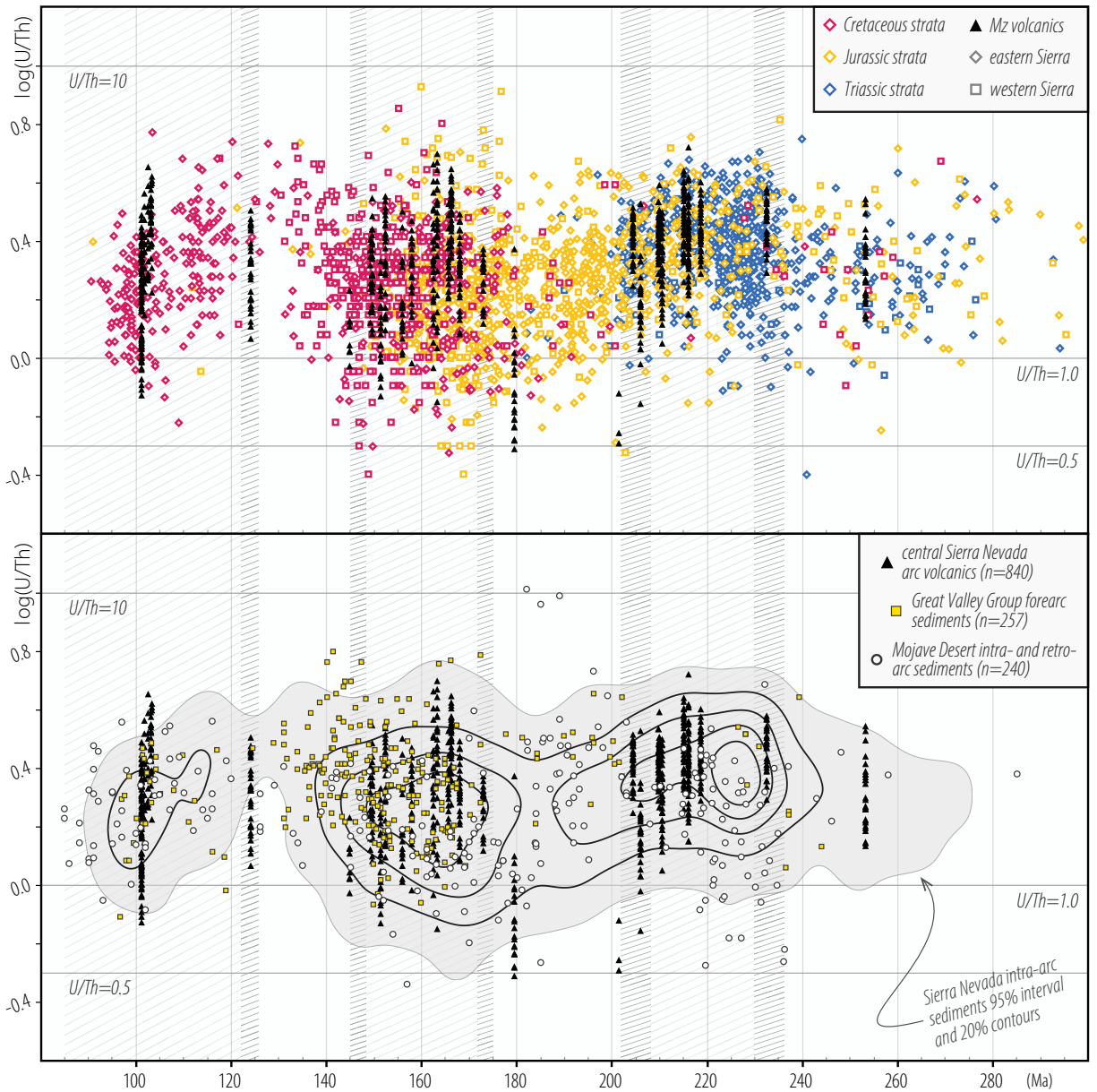

Figure 8. Comparison of U/Th values for Sierra Nevada detrital zircon analyses between 80 and 300 Ma (n = 2111), broken out by geography and depositional age, to detrital zircon analyses from Mesozoic strata in the Mojave desert, erupted zircon analyses from central Sierra Nevada Mesozoic metavolcanic rocks, and forearc deposits of the Great Valley Group (Barth et al., 2004; Riggs et al., 2013; Stone et al., 2013; Paterson et al., 2017; Surpless et al., 2019; Attia et al., 2020). Hatched intervals indicate arc flare-up timing. Mz—Mesozoic.

detrital age component together across all Sierra Nevada intra-arc strata. This complex spread of pre–300 Ma ages in intra-arc strata is nearly indistinguishable from (1) the composite detrital zircon age distribution of prebatholithic framework strata, with nearly identical age peak locations and significant overlap in U/Th values (Fig. 7), as well as (2) the composite detrital age distribution of Neoproterozoic to Lower Permian strata of the southwestern Laurentian continental margin (e.g., Owens Valley group strata, Fig. 9; Attia et al., 2018), and (3) pre-Mesozoic detrital zircon ages in Mesozoic sediments of the Cordilleran foreland (Laskowski et al., 2013). Taken together, this multimodal spread of older ages is indicative of recycling of older ages from southwestern Cordilleran margin strata. Precambrian detrital ages were originally derived from Laurentian cratonic domains, whereas latest Neoproterozoic–Paleozoic ages may have been derived from circum-Laurentian arc and orogenic provinces such as the Appalachian, Franklinian, and Ouachita orogenies or displaced slices of such assemblages introduced into the western Laurentian margin in the Paleozoic (Colpron and Nelson, 2009; Thomas, 2011; Gehrels and Pecha, 2014; Attia et al., 2018). Potential sources of recycled sediments include Sierra Nevada prebatholithic framework strata, Neoproterozoic–Paleozoic southwestern Laurentian continental margin strata, and Mesozoic foreland strata of the continental interior. While the specific source of Precambrian–Paleozoic detrital ages in Sierra Nevada intra-arc strata is ambiguous, this spread of pre–300 Ma ages is consistent with a broad western Laurentian provenance and proximity to the southwestern Cordilleran margin (Attia et al., 2018).

A limited population of 79 filtered analyses of inherited zircons in Mesozoic metavolcanic rocks of the CSN spans the same range of Precambrian–Paleozoic ages and U/Th values as pre–300 Ma detrital zircons in Sierra Nevada intra-arc strata (Fig. 7; Attia et al., 2020). A subset of inherited Paleozoic zircons with corresponding Lu-Hf isotopic analyses shown in Figure 10 are of particular interest. Initial Hf isotopic compositions of these inherited zircons span intermediate to evolved isotopic compositions (Fig. 10), indicating at least some incorporation of ancient lithospheric material in the parental magma sources of these zircons. These values fall within the range of the isotopic compositions of Paleozoic detrital zircons found in Permian–Triassic strata in the Nevada-Utah shelf, Sonoran Desert, and British Columbia as well as mid-Paleozoic basins associated with the Appalachian and Franklinian orogens (Gehrels and Pecha, 2014, and sources therein). The isotopic compositions of this inherited zircon component in CSN metavolcanic rocks can only rule out fringing arcs built into oceanic crust with no influence from continental crust as possible sources for these Paleozoic

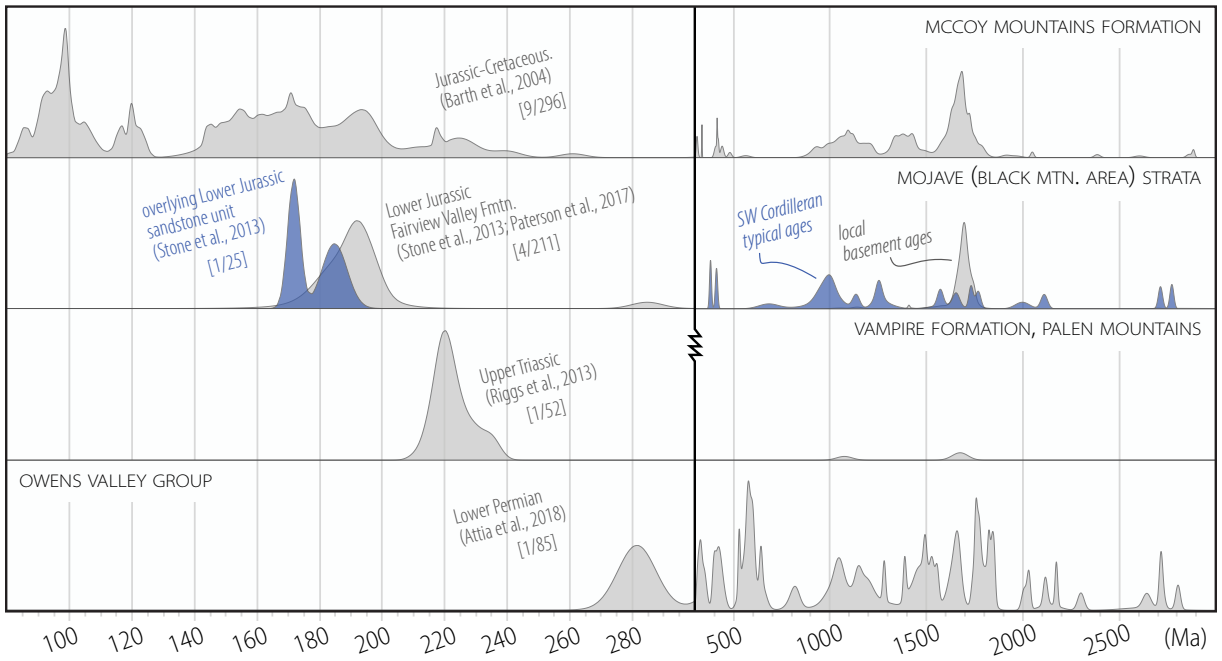

Figure 9. Summary of Mojave Desert and Owens Valley detrital zircon data. Probability density plots of detrital zircon ages from Lower Permian southwestern Laurentian continental margin, Upper Triassic retroarc, Lower Jurassic intra-arc, and Jurassic–Cretaceous retroarc basin strata.

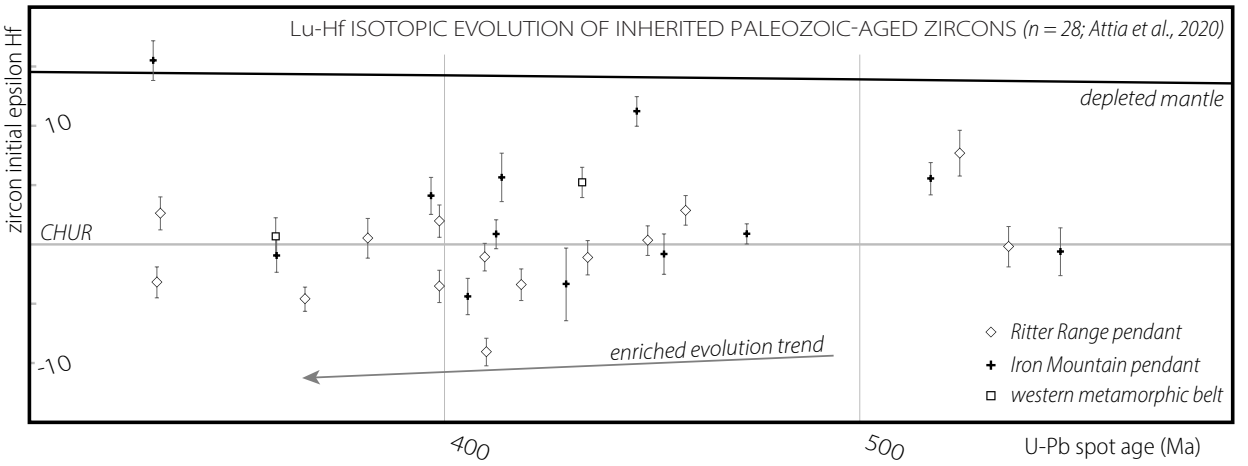

Figure 10. Zircon Lu-Hf isotopic evolution of inherited Paleozoic ages from central Sierra Nevada Mesozoic metavolcanic rocks. CHUR—CHondritic Uniform Reservoir.

detrital ages, providing the best available, but still speculative and equivocal, constraint on the provenance of Paleozoic detrital ages found in intra-arc strata.

Permian–Cretaceous Detrital Ages

Middle to Late Permian detrital zircon ages are dominantly found in Permo-Triassic strata of the eastern Sierra Nevada and central WMB as well as a few Upper Triassic samples (Fig. 6). Igneous activity of this age is found in the Sonora segment of the early Cordilleran arc system, the El Paso terrane in the northern Mojave Desert and southern Sierra Nevada, the Northern Sierra terrane, and arc rocks in western Nevada (Harwood, 1992; Miller et al., 1995; Riggs et al., 2013; Saleeby and Dunne, 2015; Christe et al., 2018; Cecil et al., 2019). The U/Th values of Middle Permian detrital zircons in Sierra Nevada strata overlap with U/Th values of erupted zircons in a Permo-Triassic volcanic sample from the central WMB, zircons in Permian plutons of the El Paso terrane, Permian detrital zircons in the Triassic retroarc Waterman Formation, and zircons in Sonoran igneous arc rocks (Fig. 8; Riggs et al., 2013; Saleeby and Dunne, 2015; Cecil et al., 2019; Attia et al., 2020).

Late Triassic detrital zircon ages are dominantly found in Upper Triassic and Lower Jurassic strata across the Sierra Nevada (Fig. 6). Arc activity of this age is well represented across the southwestern Cordilleran margin, with coeval igneous arc rocks preserved in the eastern Sierra Nevada, western Nevada Pine Nut assemblage, eastern CSN, Kern Plateau, southern Mojave Desert, and Transverse Ranges (Kistler and Ross, 1990; Bateman, 1992; Miller et al., 1995; Barth et al., 1997, 2011, 2012, 2018; Barth and Wooden, 2006; Proffett and Dilles, 2008; Klemetti et al., 2014; Cao et al., 2015; Saleeby and Dunne, 2015). U/Th values of Triassic detrital zircons in Sierra Nevada strata (~1.0–6.0) are consistent with zircon U/Th values in coeval CSN volcanic rocks and Mojave Desert plutons as well as the upper range of detrital zircon U/Th values in intra- and retro-arc strata of the Mojave Desert (Fig. 8; Barth et al., 2013; Riggs et al., 2013; Stone et al., 2013; Paterson et al., 2017; Attia et al., 2020).

Early Jurassic detrital zircon ages are dominantly found in Lower Jurassic strata across the entire Sierra Nevada (Figs. 6 and 8). Preserved igneous rocks of Early Jurassic age are rare in the Sierra Nevada, restricted to minor volcanic layers in the Mount Morrison and Mineral King pendants as well as intrusive and volcanic rocks in the central belt of the WMB (Saleeby, 1982, 2011; Edelman and Sharp, 1989; Bateman, 1992; Klemetti et al., 2014; Barth et al., 2018). Some arc rocks in the Black Rock terrane of western Nevada may also be mid-Early Jurassic in age (Christe et al., 2018). U/Th values in Early Jurassic detrital zircons in Sierra Nevada strata broadly overlap with detrital zircon U/Th values of Mojave Desert strata (Fig. 8) and zircons analyzed from Early Jurassic plutons in the Mojave Desert by Barth et al. (2017). Middle to Late Jurassic detrital zircon ages, matching the timing of the Jurassic arc flare-up, are found in Middle to Upper Jurassic, lowermost Cretaceous, and mid-Lower Cretaceous intra-arc strata (Figs. 3, 6, and 8). Detrital zircon U/Th values of Middle to Late Jurassic-aged analyses overlap erupted zircon U/Th values of CSN metavolcanics but cover a greater range toward U/Th values as low as 0.5 (Fig. 8). Such lower zircon U/Th values (~0.5–1.5) are present in detrital zircon populations from Mojave Desert strata (Fig. 8), bedrock zircons from Sierra Nevada Jurassic arc rocks, and mid-Jurassic plutons of the Mojave Desert (Barth et al., 2017; Surpless et al., 2019).

Detrital zircons of earliest to mid-Early Cretaceous age, uncommon in Sierra Nevada intra-arc strata, show U/Th values that overlap with analyses from Great Valley Group fore-arc strata (Fig. 8). Arc rocks of this age are rarely preserved in the Sierra Nevada (Fig. 3) and Mojave Desert, but geochronology from the westernmost WMB, Tehachapi Mountains, and subsurface drill cores from the eastern Central Valley, as well as the Mount Goddard and Mineral King pendants, indicates that at least some arc activity continued at this time (Saleeby et al., 1989; Saleeby, 2007; Chapman et al., 2012; Kirsch et al., 2016; Surpless et al., 2019). Detrital zircons of mid-Cretaceous age dominate detrital age distributions of mid-Lower to mid-Cretaceous Sierra Nevada strata (Fig. 6) and show U/Th values that overlap with erupted zircons from CSN metavolcanics and detrital zircons from Mojave Desert retro-arc strata and Great Valley Group fore-arc strata (Fig. 8).

Detrital Zircon Provenance

Permo-Triassic Strata

Few exposures of Upper Permian to Middle Triassic strata have been identified across the Sierra Nevada, due to either a lack of preservation or a period of nondeposition related to tectonism associated with the latest Paleozoic assembly of the Sierra Nevada prebatholithic framework (Rains et al., 2012; Saleeby and Dunne, 2015). Permo-Triassic sedimentary strata show the typical spread of Precambrian–Paleozoic ages and a Middle-Late Permian youngest detrital age peak (Fig. 6). While Permian magmatic activity is not well represented in the Sierra Nevada rock record, such detrital zircon ages are consistent with derivation from several potential sources across the earliest arc established along the southwestern Cordilleran margin (Riggs et al., 2013; Cecil et al., 2019).

Triassic Strata

Terrestrial to shallow-marine Triassic strata unconformably overlying prebatholithic framework strata are widespread inboard of the Foothills suture, except in pendants associated with the Snow Lake terrane where the regional unconformity basal to intra-arc deposits extends into the Early Jurassic (Figs. 11B and 11C). Triassic strata outboard of the Foothills suture are limited to parts of the basinal Calaveras complex and deep-marine deposits of the WMB central belt assemblages, as well as their southern equivalents. Triassic sediments of the eastern CSN Koip sequence and WMB, including strata on both sides of the Foothills suture, show largely unimodal detrital age distributions with no variation by geography or tectonostratigraphic division (Figs. 2, 4, 6, 11B, and 11C). Koip sequence strata were likely sourced from proximal arc volcanic centers and exhumed Triassic plutonic rocks attested to by granitoid lithic fragments found in Upper Triassic Cooney Lake conglomerate beds reported by Cao et al. (2015).

Upper Triassic sediments in the southern Sierra Nevada, including the eastern facies of the lower Kings sequence, show multimodal distributions with significant proportions of pre–300 Ma detrital ages (Figs. 2, 4, 6, and 11B). These sediments were likely sourced from a combination of proximal arc activity, such as that recorded in the eastern Sierra Nevada and Mojave Desert, and recycling from older Proterozoic–Paleozoic strata present across the southwestern Cordillera. In comparison, Triassic retro-arc strata including the Vampire, Waterman, and Chinle formations, show both unimodal and multimodal detrital age distributions (Fig. 9; Dickinson and Gehrels, 2010; Riggs et al., 2013, 2016). Prebatholithic framework strata are a potential source of these older recycled ages as the Permian–Triassic unconformity extends into Late Triassic time across the southern Sierra Nevada. Given the presence of both unimodal and multimodal detrital age distributions in proximal to distal retro-arc strata, we cannot rule out contributions to Sierra Nevada intra-arc strata from autochthonous southwestern Laurentian strata inboard of the arc or Precambrian–Paleozoic strata of the Mojave facies along strike of the margin.

Jurassic Strata

Lower Jurassic strata in the northern and central Sierra Nevada, including the Sailor Canyon Formation, Sawmill Canyon sequence, and Oakhurst pendant strata, show both unimodal and multimodal detrital age distributions (Figs. 6 and 11D). Strata in the axial and southern Sierra Nevada show only multimodal distributions throughout the early Mesozoic (Figs. 11B–11D). A subsidiary Late Triassic detrital age component is evident in both groups of Lower Jurassic strata (Fig. 6). In the northern Sierra Nevada, Lower Jurassic sediments of the uppermost Big Valley sequence with unimodal distributions stratigraphically underlie Lower Jurassic sediments of the Ellis Peak Formation with multimodal distributions (Christe et al., 2018). This shift is broadly coeval with a transition from shallow- to deep-marine deposition (Fig. 4). In the eastern CSN, no clear stratigraphic relationship is apparent among shallow-marine sediments of the Sawmill Canyons sequence that show unimodal versus multimodal detrital age distributions (Fig. 5A). In the southern Sierra Nevada, both deep- and shallow-marine strata of the upper Kings sequence show multimodal detrital age distributions (Fig. 11D). In comparison, Lower Jurassic intra-arc sediments of the Mojave Desert show an upsection shift from a bimodal detrital age distribution with age peaks at ca. 190 Ma and 1700 Ma to a multimodal distribution with Early Jurassic detrital ages and a spread of pre-Mesozoic ages (Fig. 9). This shift in Mojave intra-arc strata is not accompanied by any marked changes in broad depositional environment (Stone et al., 2013).

Given the geographic variation in the timing of and relationships between Early Jurassic lithostratigraphic and detrital provenance shifts described above, it appears that the Late Triassic–Early Jurassic and Precambrian–Paleozoic detrital age components in Lower Jurassic strata are derived from geographically distinct sources. Late Triassic–Early Jurassic detrital ages in Lower Jurassic strata show U/Th ratios that overlap with zircons from CSN metavolcanics

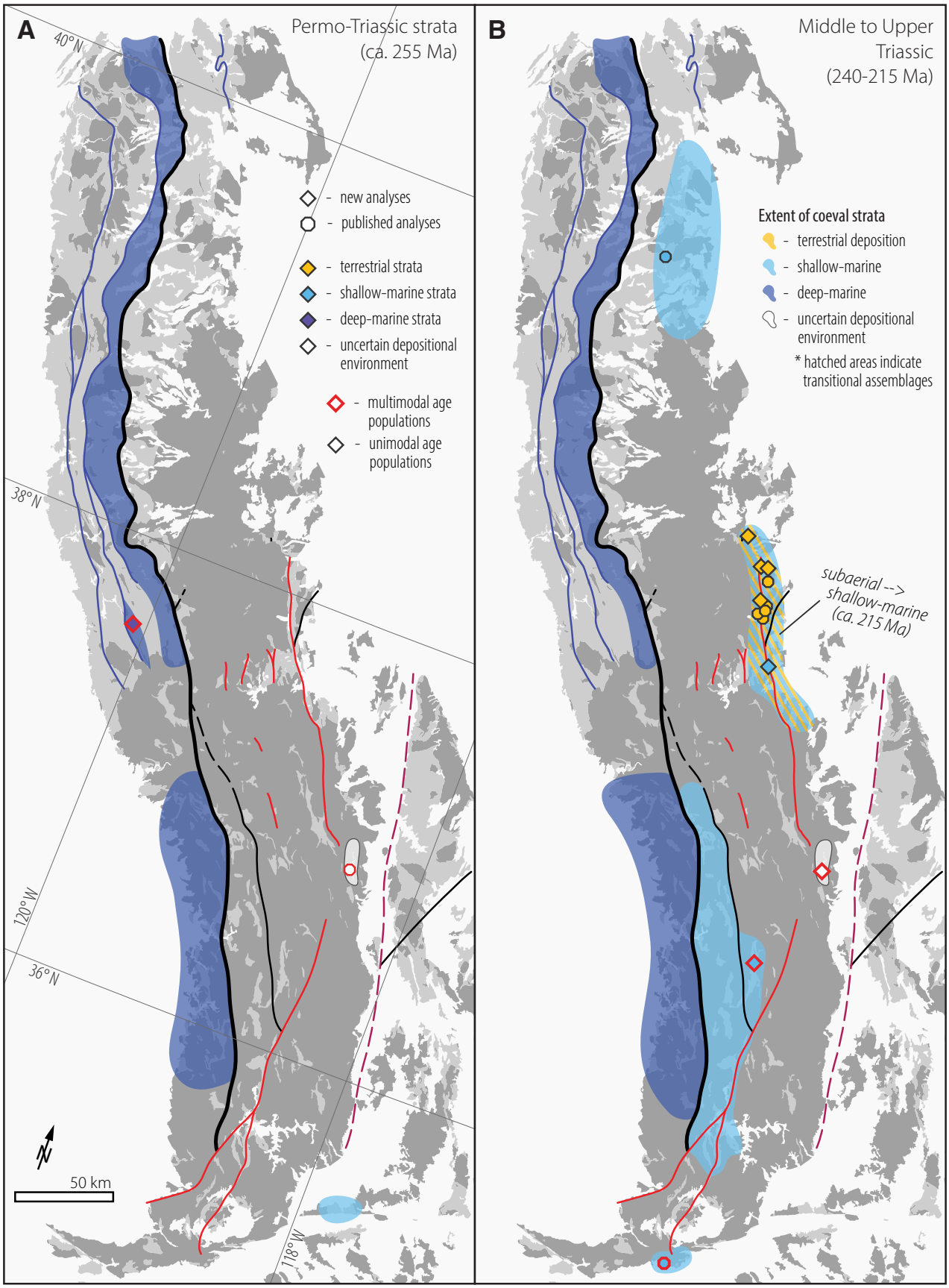

Figure 11. Summary of Sierra Nevada arc stratigraphic records and detrital zircon sample ages with panels A–H representing successive time slices. Color-shaded regions indicate aerial extent and broad depositional environment of preserved strata at each time slice based on geochronology, fossil ages, and proposed stratigraphic relationships. Map extent, faults, and generalized geology same as in Figures 1 and 2. (*Continued on following three pages.*)

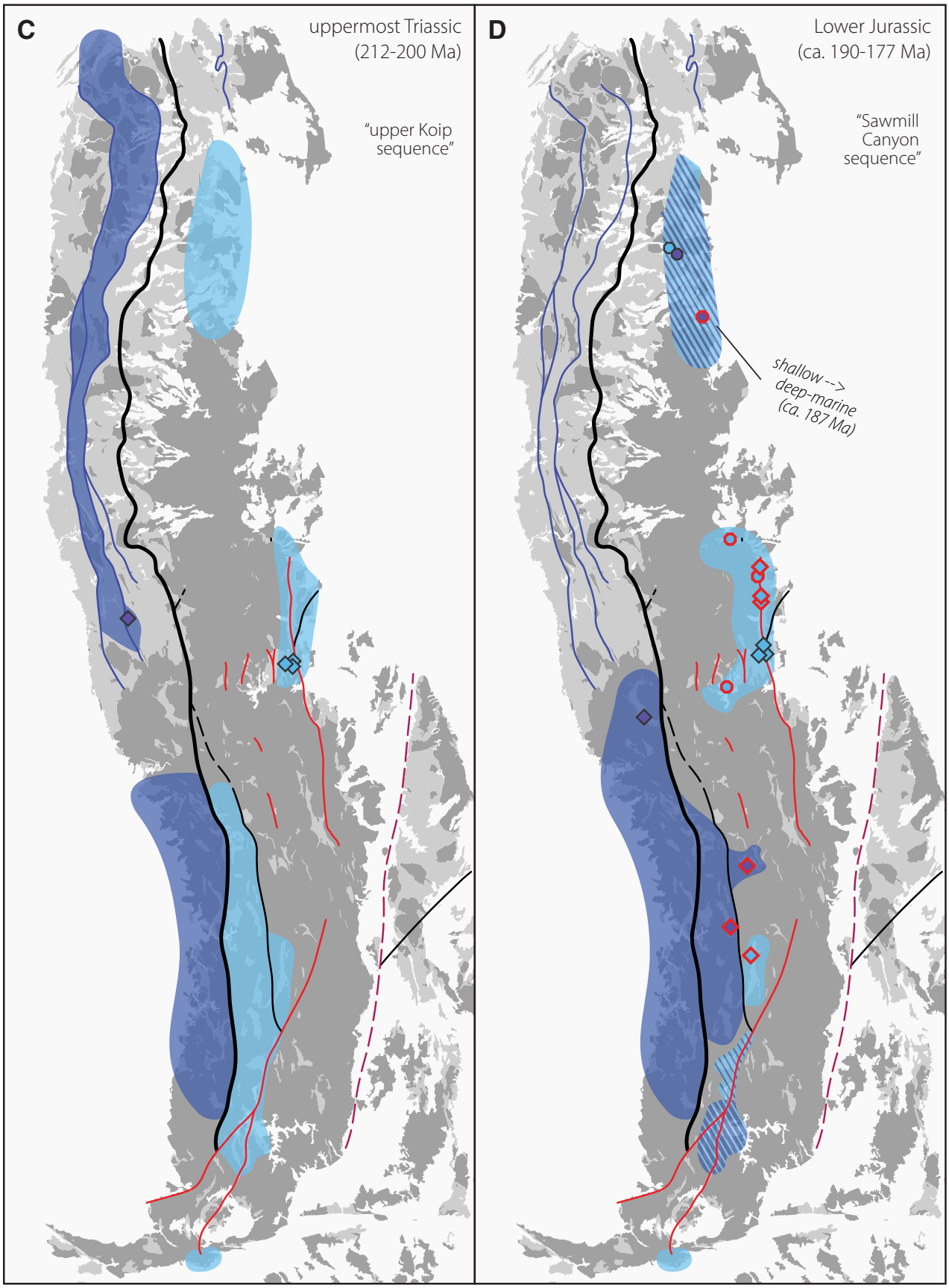

Figure 11 (*continued*). (*Continued on following two pages.*)

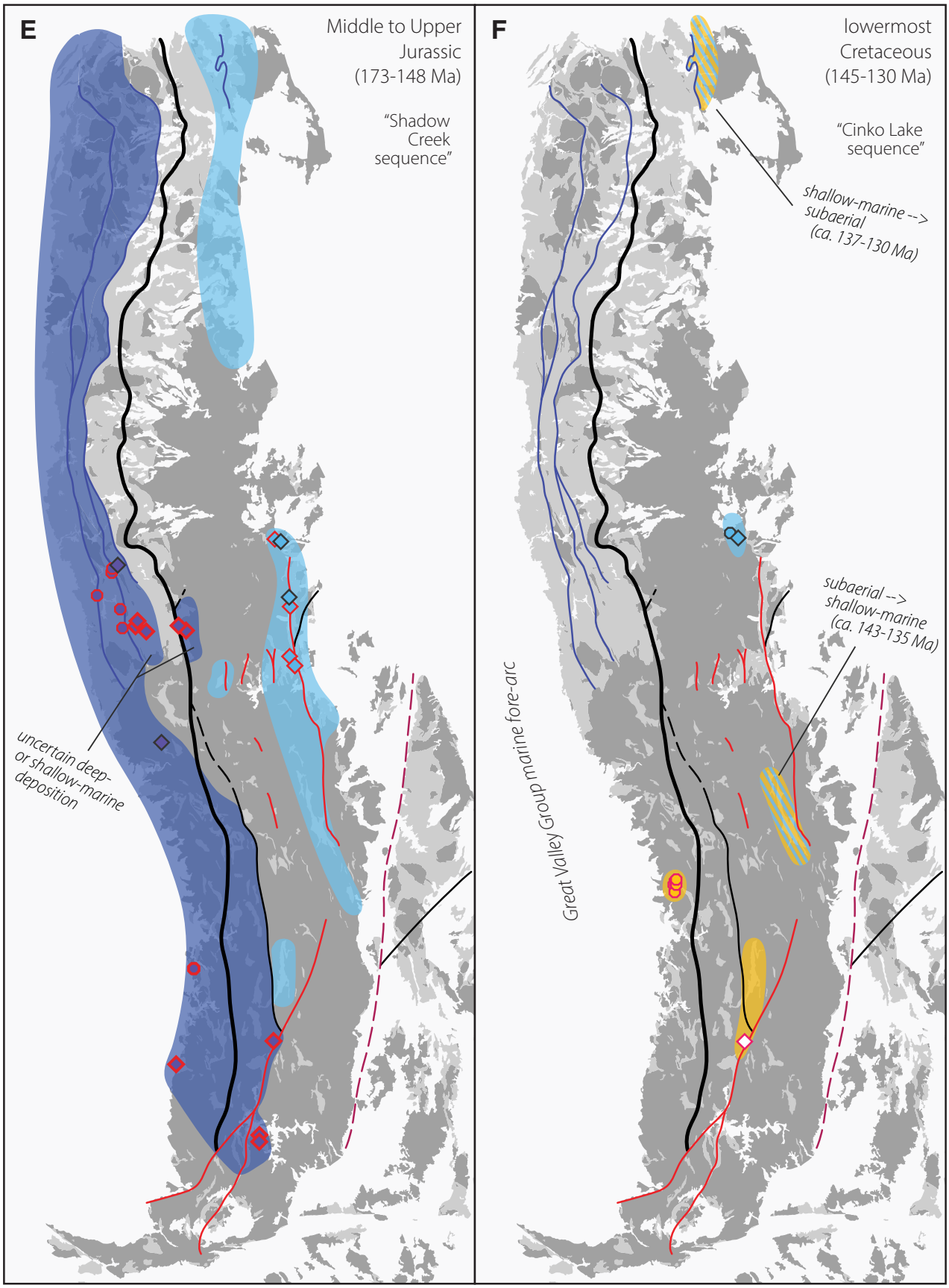

Figure 11 (*continued*). (*Continued on following page*.)

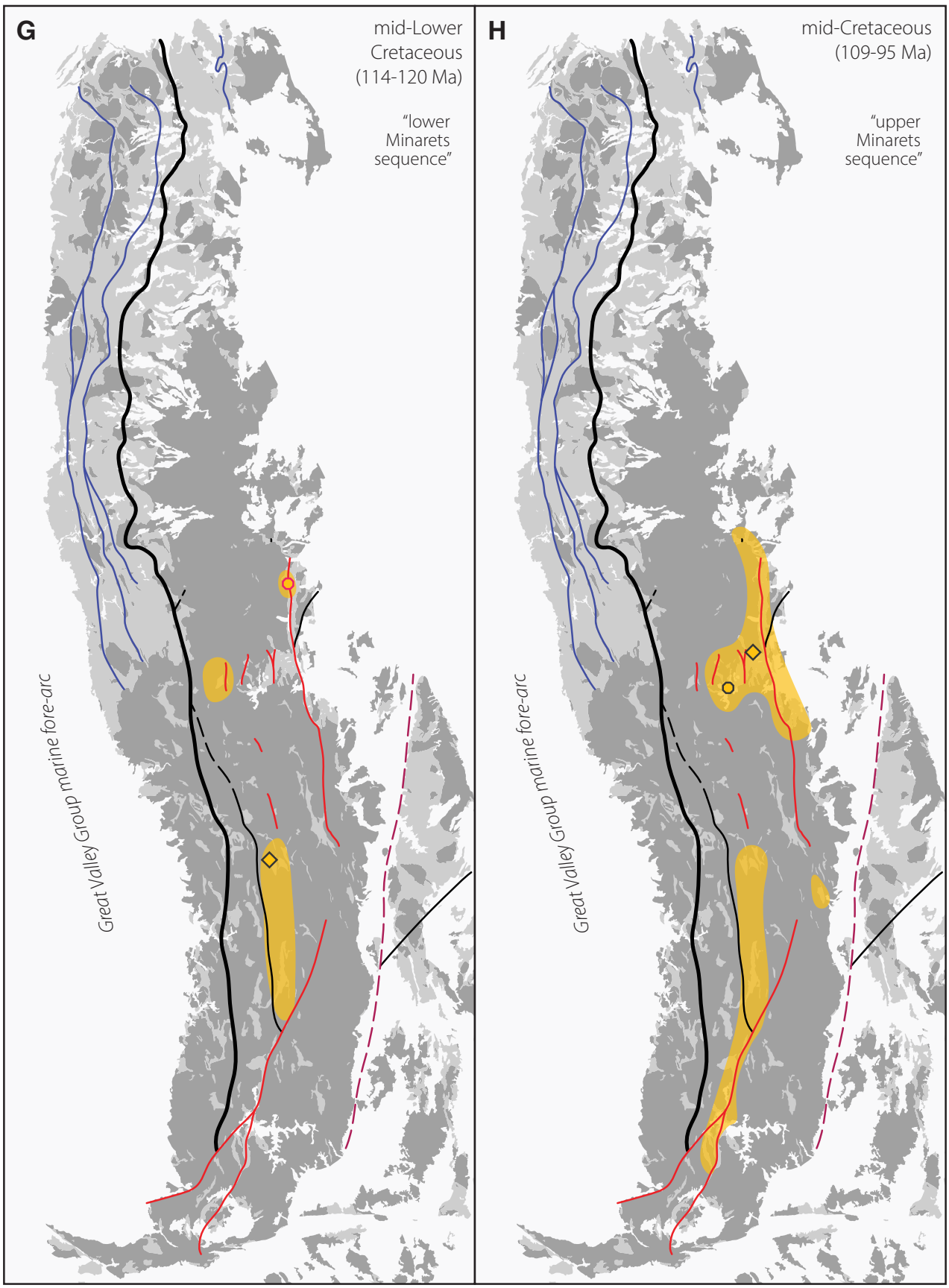

Figure 11 (*continued*).

(Fig. 8), consistent with proximal derivation from isolated Early Jurassic volcanic centers and Triassic arc rocks in the Sierra Nevada. The introduction of Precambrian–Paleozoic detrital ages into intra-arc depositional centers of the northern and central Sierra Nevada and Mojave Desert in Early Jurassic time is likely related to some change in the broader southwestern Cordilleran depositional system, potentially corresponding to Early Jurassic tectonism east of the Sierra Nevada (Dunne and Walker, 2004). The above observations and interpretations could also be consistent with previously proposed large-magnitude, Early Jurassic extension along the outboard southwestern Cordilleran margin (Busby-Spera, 1988; Saleeby and Busby, 1993; Saleeby and Dunne, 2015). In such a model, widespread intra-arc extension would have established new dispersal systems that linked low-lying intra-arc sedimentary sinks to local tectono-volcanic uplifts and newly denuded topographic highs in the Cordilleran interior.

Middle to Upper Jurassic intra-arc strata deposited in both shallow- and deep-marine environments show similar detrital age distributions across the entire Sierra Nevada, with mid-Jurassic detrital age peaks that correspond to the timing of Jurassic arc activity (Figs. 2, 4, 6, and 11E). These Jurassic ages likely reflect proximal arc activity, but some may have been sourced from the Mojave segment of the arc (Fig. 8). The source of recycled Precambrian–Paleozoic ages in these strata is again equivocal. Because preserved Early to Late Jurassic marine depositional centers span the Sierra Nevada (Fig. 6), local derivation from prebatholithic framework strata would require differential uplift of the arc surface due to tectonism and magmatism (e.g., volcanic loading). On the other hand, Jurassic detrital ages are found in most samples of Jurassic strata of the Cordilleran interior (Dickinson and Gehrels, 2010), and it is unclear how autochthonous southwestern Laurentian strata buried by these sediments could have contributed detritus to the outboard arc. Thus, we favor either a link to depositional systems of the Cordilleran interior or recycling of these older ages from lower to mid-Mesozoic sediments of the Cordilleran foreland.

Cretaceous Strata

Lowermost Cretaceous strata show similar detrital age distributions to Middle to Upper Jurassic strata, except that major age peaks are shifted toward younger Late Jurassic to earliest Cretaceous ages (Figs. 6 and 11F). Jurassic to earliest Cretaceous ages could be entirely derived from the Sierra Nevada arc or recycled from older Mesozoic intra-arc strata as parts of the arc were actively eroding in the earliest Cretaceous (Fig. 3; Martin and Clemens-Knott, 2015). Mid-Lower Cretaceous to lowermost Upper Cretaceous intra-arc metasedimentary rocks intercalated within volcanic-rich, terrestrial sequences are dominated by Early to mid-Cretaceous detrital zircon ages likely sourced from voluminous arc activity during the Cretaceous arc flare-up (Figs. 6, 8, 11G, and 11H). These dominantly unimodal Cretaceous ages stand in contrast with the multimodal detrital zircon distributions of Great Valley Group forearc strata and McCoy Mountains Formation retro-arc strata, which span Cretaceous to Proterozoic ages (Figs. 8 and 9).

Tectonostratigraphic Synthesis

In summary, Sierra Nevada intra-arc strata show provenance trends that generally shift with respect to depositional age rather than geography or tectonostratigraphic divisions, with detrital ages indicating pervasive depositional links along- and across-strike of the Sierra Nevada throughout the Mesozoic (Figs. 4, 6, and 11). Sparse Permo-Triassic strata in the Mount Pinchot pendant and structural blocks along the Melones fault zone in the WMB are broadly coeval with Upper Permian strata in the El Paso Mountains and Permian–Triassic strata of the Calaveras complex (Bateman et al., 1985; Martin and Walker, 1995; Attia et al., 2018, 2020), suggestive of a disrupted assemblage related to earliest phase of arc activity (Figs. 4 and 11A). A Permo-Triassic basaltic andesite along the Melones fault zone shows zircons with intermediate to evolved initial Hf isotopic values (Fig. 3B) that overlap with analyses from Permian plutons of the El Paso Mountains, requiring at least some input from an ancient, enriched source into the earliest Sierra Nevada arc magmatic systems (Cecil et al., 2019; Attia et al., 2020). In the Triassic, the eastern CSN represented a prominence that likely shed detritus into surrounding basins of the Koip and Big Valley sequences. Lower Kings sequence strata of the southern Sierra Nevada also received detritus from either local topographic highs or other arc segments and the Cordilleran interior (Figs. 6 and 11B). Uppermost Triassic to Lower Jurassic unconformities seen in both the central and northern Sierra Nevada correspond to the unconformity observed locally between the lower and upper Kings sequence (Fig. 4).

No later than the Middle Jurassic, but possibly as early as the earliest Jurassic, an inter-connected marine depositional system was established across the entire Sierra Nevada with water depth increasing westwards (Fig. 11D). This depositional system is preserved as the Sawmill Canyon and Shadow Creek sequences in the eastern CSN, the marine cover of the Snow Lake terrane in the axial Sierra Nevada, the Sailor Canyon Formation and correlative units to the north, and the upper Kings sequence in the south. Given similarities in lithostratigraphic and detrital zircon provenance trends, we propose to extend the Sawmill Canyon sequence of the eastern CSN to include all Lower Jurassic marine strata overlying the Snow Lake terrane. In the WMB, Middle to Upper Jurassic strata coeval with the Shadow Creek sequence unconformably overlie Permian to Lower Jurassic deposits. East of the Melones fault zone, these strata are in-folded or faulted into older Permian to Lower Jurassic deposits. It is unclear whether this overlap assemblage represents a single, contiguous sedimentary apron punctuated by volcanic centers or a series of distinct intra-arc basins with shared provenance.

We herein group all lowermost Cretaceous strata across the Sierra Nevada into the informal Cinko Lake sequence, including the terrestrial deposits of the Goldstein Peak Formation and broadly coeval strata in the northeastern-most Sierra Nevada (Christe, 2014). Earliest Cretaceous isolated, shallow-marine to terrestrial depositional centers, coeval with a widespread unconformity following extensive Late Jurassic contraction (Figs. 3 and 11F), indicate differential uplift as the arc transitioned to an emergent surface expression and

shed sediments into the nascent Great Valley Group forearc basin (Orme and Surpless, 2019). The local persistence of marine depositional environments in the Sierra Nevada into the earliest Cretaceous and the overlap in zircon U/Th values between intra- and fore-arc strata is inconsistent with the mismatch in trace-element compositions between fore-arc detrital zircons and eastern CSN arc rocks proposed by Surpless et al. (2019), on the basis of which they proposed the existence of an intra-arc east-west drainage divide as early as Jurassic–Cretaceous time. Mid-Lower to lower Upper Cretaceous strata were deposited above a profound Jurassic to Lower Cretaceous angular unconformity across the entire central and southern Sierra Nevada (Fig. 4), and we herein group all of these terrestrial, volcanic-dominated packages into the informal Minarets sequence.

Mesozoic Terranes in the Sierra Nevada

Previous workers have proposed that fault-bounded belts and assemblages in the northern and central WMB represent exotic terranes and/or oceanic arcs accreted against the Sierra Nevada during a punctuated Late Jurassic Nevadan orogeny (e.g., Hamilton, 1969; Moores, 1970; Schweickert and Cowan, 1975; Schweickert et al., 1984; Dickinson, 2008). Others have viewed these WMB arc and volcanic assemblages as native to the outboard margin of the Sierra Nevada and interpreted the structural-stratigraphic complexity as protracted Jurassic deformation within the arc (e.g., Burchfiel and Davis, 1972; Edelman et al., 1989; Paterson et al., 1989; Tobisch et al., 1989; Day and Bickford, 2004). None of the detrital zircon data presented herein require that any Mesozoic Sierra Nevada strata are part of exotic terranes or outboard oceanic arcs accreted against the margin in Mesozoic time.

The compiled detrital zircon age data indicate that strata west of the Foothills suture were part of the same Permo-Triassic to Cretaceous sedimentary dispersal system as strata of the axial and eastern Sierra Nevada, with direct depositional links to the southwestern Cordilleran margin (Figs. 2, 6, 8, and 11). Jurassic strata on both sides of the Melones fault zone show multimodal detrital age distributions with indistinguishable Precambrian–Paleozoic components and overlapping depositional ages (Figs. 2, 4, and 10). This contradicts terrane and/or arc accretion models, which would predict that at least some of the sedimentary strata associated with accreted assemblages would show unimodal detrital age distributions or multimodal distributions with pre-Mesozoic components exotic to the southwestern Cordilleran margin. The Triassic–Jurassic Fiddle Creek complex, Slate Creek complex, and Penon Blanco arc assemblage represent the only potential accreted Mesozoic arcs, but it is important to note that no data require such accretion. It is equally likely that these rocks represent outboard, forearc magmatism built over the same west-facing subduction zone as the rest of the arc (Saleeby and Busby, 1993).

Furthermore, intermediate to evolved isotopic signatures in Permo-Triassic to Late Jurassic arc rocks in the WMB require some evolved component in western Sierra Nevada magmas, indicating involvement of continental material that was either derived from, or was itself part of, the southwestern Cordillera (Saleeby, 1982; Day and Bickford, 2004; Attia et al., 2020). Latest Triassic to Late Jurassic WMB arc assemblages were built into deformed ophiolitic and basinal basement rocks already part of the Sierra Nevada framework, and thus represent the western extent of Sierra Nevada–wide Jurassic magmatic activity coeval with long-lived tectonism spanning Middle to Late Jurassic time (Saleeby, 1982; Edelman et al., 1989; Tobisch et al., 1989). This broad, native arc likely experienced structural disruptions, but these occurred within the supra-subduction environment that was established after the late Paleozoic assembly of the prebatholithic framework along the southwestern Cordilleran margin (Chapman et al., 2015; Saleeby and Dunne, 2015). Combined with our compiled detrital zircon age data, previously established geologic relationships preclude models that envisage Middle to Late Jurassic assemblages in the WMB as exotic, accreted arcs (cf. Schweickert et al., 1984; Schweickert, 2015; Sigloch and Mihalyunk, 2017).

Intra-Batholithic Transform Faults

Tectonostratigraphic constraints synthesized with detrital zircon data are also inconsistent with the existence of major Mesozoic intrabatholithic transforms with displacements of hundreds of kilometers (e.g., Schweickert and Lahren, 1990) that are proposed to have dispersed strata across the southwestern Cordilleran margin. Triassic strata overlying the Paleozoic Northern Sierra terrane are proposed to have been originally deposited near the El Paso terrane and then translated northwards in the latest Triassic on the basis of lithostratigraphic trends and limited detrital zircon age data (Christe et al., 2018). The provenance links proposed by Christe et al. (2018) between Triassic marine strata of the northern WMB eastern belt and El Paso terrane rocks are non-unique because Middle to Late Permian detrital ages are present in other Permo-Triassic to Upper Triassic strata of the Sierra Nevada (Fig. 6). Similarly, Triassic–Jurassic strata in the northern Sierra Nevada show detrital provenance and stratigraphic trends consistent with the rest of the Sierra Nevada (Figs. 4 and 11B–11E). Thus, no Mesozoic displacements along hypothetical cryptic structures separating the northern Sierra Nevada from the rest of the arc are required.

The Neoproterozoic–Paleozoic Snow Lake terrane and overlying Lower Jurassic strata are proposed to have originally been deposited in the Mojave area, on the basis of stratigraphic correlations and limited detrital zircon age data, prior to subsequent northwards displacement to their current positions within the axial Sierra Nevada during the Mesozoic (e.g., Schweickert and Lahren, 1990). Despite these proposed correlations, the stratigraphy and detrital provenance of the Snow Lake terrane is just as consistent with coeval southwestern Laurentian continental margin strata spanning northern Mexico to Idaho as with the Mojave Desert miogeocline (Attia et al., 2018). Furthermore, detrital zircon ages of the marine strata unconformably overlying the Snow Lake terrane are much more similar to detrital ages of proximal Sierra

Nevada strata than Mojave Desert terrestrial deposits (Figs. 4, 6, and 9). In addition, Lower Jurassic strata in the Mojave Desert unconformably overlie Mesoproterozoic–Paleozoic strata that are intruded by a suite of Triassic plutons, whereas no Triassic arc rocks are associated with the Snow Lake terrane (Bateman, 1992; Stone et al., 2013). Thus, the proposed correlations between Lower Jurassic strata overlying the Snow Lake terrane and coeval Mojave Desert strata are herein rejected. Because no evidence attests to or requires the existence of a Mojave–Snow Lake fault (Memeti et al., 2010; Chapman et al., 2015; Saleeby and Dunne, 2015), we reject the existence of this hypothesized Mesozoic intra-batholithic transform and the attendant 100-km-scale, intra-arc displacements.

CONCLUSIONS

Sierra Nevada Arc Evolution

The Permian to Cretaceous surface history of the Sierra Nevada consists of:

(1) Deposition of a Permian–Triassic sedimentary assemblage across at least some of the southern Sierra Nevada followed, or was coeval with the final stages of, the late Paleozoic juxtaposition of the prebatholithic framework terranes along the southwestern Cordilleran margin (Figs. 4 and 11A). This assemblage shows clear provenance links with the southwestern Cordilleran margin and was associated with the earliest phase of Cordilleran arc magmatism and Late Permian basinal sediments accreted outboard of the Foothills suture. The broadly coeval, regional Permian–Triassic unconformity is a much more prominent Sierra Nevada–wide feature.

(2) In the Late Triassic, a continental arc was well established and undergoing the first of three arc flare-ups. The arc surface was dominated by shallow-marine depositional settings coeval with continued basinal sedimentation outboard of the Foothills suture (Figs. 4 and 11B). Southern intra-arc basins received pre-Mesozoic detrital zircons that were likely recycled from Neoproterozoic–Paleozoic strata of the southwestern Cordilleran margin. Terrestrial strata were deposited as aprons around major volcanic centers in the eastern CSN that formed isolated topographic highs and shed arc-derived detritus into proximal subaerial basins and surrounding marine basins. Triassic plutons intruding tilted Triassic strata in the eastern CSN and crosscutting relationships in the Mount Morrison pendant suggest a mid-Triassic tectonic event (Greene et al., 1997; Cao et al., 2015). As this arc flare-up waned in the latest Triassic, marine depositional settings dominate all stratigraphic records (Figs. 3, 4, and 11C).

(3) A latest Triassic–earliest Jurassic unconformity formed across the Sierra Nevada coeval with the waning of arc activity into a magmatic lull (Fig. 3). The latest Triassic to earliest Jurassic has been proposed to be a time of incipient extension preceding major Early Jurassic arc-normal extension (Busby-Spera et al., 1990; Saleeby and Dunne, 2015). Coeval arc activity outboard of the Foothills suture in the WMB represents either an (1) oceanic arc accreted before the mid-Early Jurassic or (2) forearc magmatic centers associated with suprasubduction extension (Edelman and Sharp, 1989; Saleeby and Busby, 1993; Day and Bickford, 2004; Saleeby, 2011). These Triassic–Jurassic volcanic assemblages are truncated by the regional unconformity that may extend into the uppermost Triassic at its base and at least into the uppermost Lower Jurassic in the WMB.

(4) As the Early Jurassic magmatic lull continued, dominantly sedimentary strata were deposited in marine environments across the Sierra Nevada by ca. 190 Ma (Fig. 4), following the final denudation of the Snow Lake terrane. Inboard parts of the arc show shallow-water depositional conditions that gave way to deep-marine environments in the northern and southern Sierra Nevada (Fig. 11D). Shallow- and deep-marine strata were deposited across the axial Sierra Nevada, with more outboard sediments apparently entirely in deep-marine basins (Behrman and Parkison, 1978; Saleeby and Busby, 1993; Saleeby, 2011). Intra-arc strata in the northern and central Sierra Nevada record a broadly coeval shift in provenance marked by the introduction of pre-Mesozoic detrital age components (Figs. 4, 6,11D, and 11E). The Early Jurassic has been proposed to be a time of significant regional extension across the southwestern Cordilleran margin, which may have also driven the tectonic emplacement and denudation of the Snow Lake terrane (Busby-Spera et al., 1990; Saleeby and Busby, 1993; Chapman et al., 2015; Saleeby and Dunne, 2015).

(5) The Sierra Nevada arc entered a second magmatic flare-up at the end of the Early Jurassic (Fig. 3). Middle to Upper Jurassic strata appear to represent an outboard-deepening, volcanic-sedimentary apron within a submarine continental arc that received sedimentary input from the retroarc foreland (Figs. 6, 8, and 11E). Observations across the arc of prolonged mid-Jurassic tectonism (Edelman and Sharp, 1989; Saleeby et al., 1989; Tobisch et al., 1989, 2000), Permo-Triassic to Upper Jurassic strata with provenance links to the southwestern Cordilleran margin, and in-folding and/or faulting of such Jurassic strata into older packages are inconsistent with previously proposed Late Jurassic accretion of outboard arcs during a punctuated Nevadan orogeny. Marine depositional environments persisted throughout this period despite high magmatic addition rates and prolonged orogenic activity spanning the Middle and Late Jurassic (Fig. 3). This disparity between expected crustal thickening and persistent marine surface conditions may be explained by exceptionally thin arc crust at the start of the Jurassic flare-up due to dramatic extension and/or root loss in the Early Jurassic (Cao and Paterson, 2016). Alternatively, the persistence of marine environments in the Jurassic arc surface may be due to the relatively low volume and diffuse nature of Jurassic magmatism, cryptic arc-parallel extension, or an exceptionally dense arc root (Paterson et al., 2019).

(6) The end of the Jurassic arc flare-up and transition into the Early Cretaceous magmatic lull were marked by the development of a Jurassic–Cretaceous unconformity across much of the Sierra Nevada (Fig. 4). Isolated exposures of lowermost Cretaceous strata deposited in shallow-marine to terrestrial environments record part of the transition of the Sierra Nevada into an emergent arc and "Andean" type orogen that likely began in the latest Jurassic (Fig. 11F).

(7) The arc transitioned into a final flare-up ca. 125–120 Ma (Fig. 3; Paterson and Ducea, 2015; Ardill et al., 2018). Intra-arc strata associated with this flare-up are poorly preserved across the Sierra and consist of dominantly volcanic sequences deposited in terrestrial environments with detrital zircon provenance dominated by coeval arc ages. Depositional ages of these strata reveal two distinct age groups preserved within the herein named Minarets sequence, one set of mid-Lower Cretaceous strata deposited ca. 120–115 Ma and upper Lower Cretaceous to lowermost Upper Cretaceous strata deposited ca. 107–98 Ma (Figs. 4 and 11G–11H). These latter strata are coeval with extensive intra-arc contraction in the eastern Sierra Nevada that transitioned to dextral transpression ca. 100 Ma (Tobisch et al., 1995; Cao et al., 2015). This ultimate flare-up culminated ca. 85 Ma with magmatism and tectonism migrating eastward into more inboard regions of the southwestern Cordilleran margin.

Links to Arc and Orogenic Tempos

The lithostratigraphic record of intra-arc depositional settings and surface processes is controlled by the impacts of arc magmatism and tectonism on the development of lithospheric architecture, with tectonic thickening and/or thinning of the lithosphere as the dominant contribution (Cao and Paterson, 2016). This may occur via controls on accommodation space at the surface of the arc due to changing lithospheric column thickness and density, dynamic mantle topography, and the influence of near-surface magmatism and deformation local relief and accommodation space. This mediation of surface evolution by the development of lithospheric architecture, which is driven by the consequences of episodic arc and orogenic processes (Cao and Paterson, 2016), subtly contrasts with direct links between intra-arc sedimentation and episodic behavior. Furthermore, parts of the Sierra Nevada were sinks for both arc-derived and external sediments throughout the Mesozoic even as the arc shed detritus into depositional centers along- and across-strike of the southwestern Cordilleran margin. Thus, geologic processes and events external to the arc also exerted control on intra-arc sedimentary provenance.

ACKNOWLEDGMENTS

Paterson gratefully acknowledges support from National Science Foundation grants EAR-1524798, 1019636, 0537892, and 0212276 and U.S. Geological Survey EDMAP grants G16AC00160, G15AC00134, G13AC00120, G12AC20178, and 08HQAG0057. National Science Foundation EAR-1338583 supported analyses at the Arizona LaserChron Center. We would like to express our immense gratitude to Arizona LaserChron Center personnel for their extensive assistance with detrital zircon geochronology analyses, which represents an invaluable contribution to this effort. We acknowledge Katie Ardill, Vali Memeti, Lawford Anderson, and undergraduate participants in the Undergraduate Team Research program for their help in collecting samples from the Ritter Range, Saddlebag Lake, and Boyden Cave pendants and central WMB as well as conducting geochronology analyses; Calvin Stevens and Paul Stone for collecting the Mount Pinchot pendant sample; Chuck Herzig for assistance during sampling along the Merced River; Elisabeth Nadin for her guidance and help during sampling in the Durrwood pendant area; and David Greene for sharing samples collected from the Mineral King pendant. We also thank editors Nancy Riggs and David Fastovksy as well as two anonymous reviewers for their efforts, which greatly improved this manuscript.

REFERENCES CITED

Ardill, K.A., Paterson, S.R., and Memeti, V., 2018, Spatiotemporal magmatic focusing in upper-mid crustal plutons of the Sierra Nevada arc: Earth and Planetary Science Letters, v. 498, p. 88–100, https://doi.org/10.1016/j.epsl.2018.06.023.

Ardill, K.E., Memeti, V., and Paterson, S.R., 2020, Reconstructing the physical and chemical development of a pluton-porphyry complex in a tectonically re-organized arc crustal section, Tioga Pass, Sierra Nevada: Lithosphere, v. 2020, no. 1, p. 1–26, https://doi.org/10.2113/2020/8872875.

Armstrong, R.L., and Ward, P.L., 1993, Late Triassic to earliest Eocene magmatism in the North American Cordillera: Implications for the Western Interior Basin, *in* Caldwell, W.G.E., and Kauffman, E.G., eds., Evolution of the Western Interior Basin: Geological Association of Canada Special Paper 39, p. 49–72.

Arvizu, H.E., and Iriondo, A., 2015, Temporal and geologic control of Permo-Triassic magmatism in Sierra Los Tanques, NW Mexico: Evidence of the initiation of cordilleran arc magmatism in SW Laurentia: Bulletin of the Geological Society of Mexico, v. 67, p. 545–586.

Attia, S., Paterson, S.R., Cao, W., Chapman, A.D., Saleeby, J., Dunne, G.C., Stevens, C.H., and Memeti, V., 2018, Late Paleozoic tectonic assembly of the Sierra Nevada prebatholithic framework and western Laurentian provenance links based on synthesized detrital zircon geochronology, *in* Ingersoll, R.V., Lawton, T.F., and Graham, S.A., eds., Tectonics, Sedimentary Basins, and Provenance: A Celebration of William R. Dickinson's Career: Geological Society of America Special Paper 540, p. 267–295, https://doi.org/10.1130/2018.2540(12).

Attia, S., Cottle, J.M., and Paterson, S.R., 2020, The erupted zircon record of continental crust formation during mantle driven arc flare-ups: Geology, v. 48, no. 5, p. 446–451, https://doi.org/10.1130/G46991.1.

Barth, A.P., and Wooden, J.L., 2006, Timing of magmatism following initial convergence at a passive margin, southwestern U.S. Cordillera, and ages of lower crustal magma sources: The Journal of Geology, v. 114, p. 231–245, https://doi.org/10.1086/499573.

Barth, A.P., Tosdal, R.M., Wooden, J.L., and Howard, K.A., 1997, Triassic plutonism in southern California: Southward younging of arc initiation along a truncated continental margin: Tectonics, v. 16, p. 290–304, https://doi.org/10.1029/96TC03596.

Barth, A.P., Wooden, J.L., Jacobson, C.E., and Probst, K., 2004, U-Pb geochronology and geochemistry of the McCoy Mountains Formation, southeastern California: A Cretaceous retroarc foreland basin: Geological Society of America Bulletin, v. 116, no. 1–2, p. 142–153, https://doi.org/10.1130/B25288.1.

Barth, A.P., Walker, J.D., Wooden, J.L., Riggs, N.R., and Schweickert, R.A., 2011, Birth of the Sierra Nevada magmatic arc: Early Mesozoic plutonism and volcanism in the east-central Sierra Nevada of California: Geosphere, v. 7, p. 877–897, https://doi.org/10.1130/GES00661.1.

Barth, A.P., Feilen, A.D.G., Yager, S.L., Douglas, J.L., Riggs, N.R., and Walker, J.D., 2012, Petrogenetic connections between ash-flow tuffs and a granodioritic to granitic intrusive suite in the Sierra Nevada arc, California: Geosphere, v. 8, no. 2, p. 250–264, https://doi.org/10.1130/GES00737.1.

Barth, A.P., Wooden, J.L., Jacobson, C.E., and Economos, R.C., 2013, Detrital zircon as a proxy for tracking the magmatic arc system: The California arc example: Geology, v. 41, no. 2, p. 223–226, https://doi.org/10.1130/G33619.1.

Barth, A.P., Wooden, J.L., Miller, D.M., Howard, K.A., Fox, L.K., Schermer, E.R., and Jacobson, C.E., 2017, Regional and temporal variability of melts during a Cordilleran magma pulse: Age and chemical evolution of the Jurassic arc, eastern Mojave Desert, California: Geological Society of America Bulletin, v. 129, no. 3–4, p. 429–448, https://doi.org/10.1130/B31550.1.

Barth, A.P., Wooden, J.L., Riggs, N.R., Walker, J.D., Tani, K., Penniston-Dorland, S.C., Jacobson, C.E., Laughlin, J.A., and Hiramatsu, R., 2018, Marine volcaniclastic record of early arc evolution in

the Eastern Ritter Range pendant, Central Sierra Nevada, California: Geochemistry, Geophysics, Geosystems, v. 19, p. 2543–2559, https://doi.org/10.1029/2018GC007456.
Bartley, J.M., Glazner, A.F., and Mahan, K.M., 2001, Structure of the Cardinal Mountain interpluton screen, Sierra Nevada batholith, California: Geological Society of America Abstracts with Programs, v. 33, no. 3, p. 48.
Bateman, P.C., 1992, Plutonism in the central part of the Sierra Nevada batholith, California: U.S. Geological Survey Professional Paper 1483, 186 p., https://doi.org/10.3133/pp1483.
Bateman, P.C., and Wahrhaftig, C., 1966, Geology of the Sierra Nevada, *in* Bailey, E.A., ed., Geology of Northern California: California Division of Mines and Geology Bulletin 190, p. 107–172.
Bateman, P.C., Busacca, A.J., and Sawka, W.N., 1983, Cretaceous deformation in the western foothills of the Sierra Nevada, California: Geological Society of America Bulletin, v. 94, p. 30–42, https://doi.org/10.1130/0016-7606(1983)94<30:CDITWF>2.0.CO;2.
Bateman, P.C., Harris, A.G., Kistler, R.W., and Krauskopf, K.B., 1985, Calaveras reversed: Westward younging is indicated: Geology, v. 13, p. 338–341, https://doi.org/10.1130/0091-7613(1985)13<338:CRWYII>2.0.CO;2.
Behrman, P.S., and Parkison, G.A., 1978, Pre-Callovian rocks, west of the Melones fault, central Sierra Nevada Foothills, *in* Howell, D.G., and McDougall, K.A., eds., Mesozoic Paleogeography of the Western United States: Pacific Section, Society of Economic Paleontologists and Mineralogists, Pacific Coast Paleogeography Symposium 2, p. 337–348.
Bhattacharyya, T., 1986, Tectonic evolution of the Shoo Fly Formation and the Calaveras complex, central Sierra Nevada, California [Ph.D. thesis]: Santa Cruz, University of California, 338 p.
Bogen, N.L., 1985, Stratigraphic and sedimentologic evidence of a submarine island-arc volcano in the lower Mesozoic Penon Blanco and Jasper Point Formations, Mariposa County, California: Geological Society of America Bulletin, v. 96, p. 1322–1331, https://doi.org/10.1130/0016-7606(1985)96<1322:SASEOA>2.0.CO;2.
Brook, C.A., 1974, Nature of the angular unconformity between the Paleozoic metasedimentary rocks and the Mesozoic metavolcanic rocks in the Eastern Sierra Nevada, California: Geological Society of America Bulletin, v. 85, p. 571–576, https://doi.org/10.1130/0016-7606(1974)85<571:NOTAUB>2.0.CO;2.
Brook, C.A., 1977, Stratigraphy and structure of the Saddlebag Lake roof pendant, Sierra Nevada, California: Geological Society of America Bulletin, v. 88, p. 321–334, https://doi.org/10.1130/0016-7606(1977)88<321:SASOTS>2.0.CO;2.
Burchfiel, B.C., and Davis, G.A., 1972, Structural framework and evolution of the southern part of the Cordilleran orogen, western United States: American Journal of Science, v. 272, p. 97–118, https://doi.org/10.2475/ajs.272.2.97.
Busby-Spera, C.J., 1988, Speculative tectonic model for the lower Mesozoic arc of the southwest Cordilleran United States: Geology, v. 16, p. 1121–1125, https://doi.org/10.1130/0091-7613(1988)016<1121:STMFTE>2.3.CO;2.
Busby-Spera, C.J., and Saleeby, J., 1987, Geologic guide to the Mineral King area, Sequoia National Park, California: Pacific Section, Society of Economic Paleontologists and Mineralogists Guidebook 56, 44 p.
Busby-Spera, C.J., Mattinson, J.M., Riggs, N.R., and Schermer, E.R., 1990, The Triassic–Jurassic magmatic arc in the Mojave-Sonoran Deserts and the Sierran-Klamath region; Similarities and differences in paleogeographic evolution, *in* Harwood, D.S., and Miller, M.M., eds., Paleozoic and Early Mesozoic Paleogeographic Relations; Sierra Nevada, Klamath Mountains, and Related Terranes: Geological Society of America Special Paper 255, p. 325–338, https://doi.org/10.1130/SPE255-p325.
Cao, W., 2016, Links, tempos, and mass balances of cyclic deformation and magmatism in arcs: A case study on the Mesozoic Sierra Nevada arc integrating geological mapping, geochronology, geobarometry, strain analyses and numerical simulations [Ph.D. thesis]: Los Angeles, University of Southern California, 413 p.
Cao, W., and Paterson, S.R., 2016, A mass balance and isostasy model: Exploring the interplay between magmatism, deformation and surface erosion in continental arcs using central Sierra Nevada as a case study: Geochemistry, Geophysics, Geosystems, v. 17, no. 6, p. 2194–2212, https://doi.org/10.1002/2015GC006229.
Cao, W., Paterson, S.R., Memeti, V., Mundil, R., Anderson, L., and Schmidt, K., 2015, Tracking paleodeformation fields in the Mesozoic central Sierra Nevada arc: Implications for intra-arc cyclic deformation and arc tempos: Lithosphere, v. 7, p. 296–320, https://doi.org/10.1130/L389.1.
Cecil, M.R., Ferrer, M.A., Riggs, N.R., Marsaglia, K., Kylander-Clark, A., Ducea, M.N., and Stone, P., 2019, Early arc development recorded in Permian–Triassic plutons of the northern Mojave Desert region, California, USA: Geological Society of America Bulletin, v. 131, no. 5–6, p. 749–765, https://doi.org/10.1130/B31963.1.
Chapman, A.D., Saleeby, J.B., Wood, D.J., Piasecki, A., Farley, K.A., Kidder, S., and Ducea, M.N., 2012, Late Cretaceous gravitational collapse of the southern Sierra Nevada batholith, California: Geosphere, v. 8, p. 314–341, https://doi.org/10.1130/GES00740.1.
Chapman, A.D., Ernst, W.G., Gottlieb, E., Powerman, V., and Metzger, E.P., 2015, Detrital zircon geochronology of Neoproterozoic–Lower Cambrian passive-margin strata of the White-Inyo Range, east-central California: Implications for the Mojave–Snow Lake fault hypothesis: Geological Society of America Bulletin, v. 127, no. 7–8, p. 926–944, https://doi.org/10.1130/B31142.1.
Christe, G., 2014, Paleogeographic implications of shallow marine to subaerial, Lower Cretaceous rocks in the eastern Mesozoic belt of northeastern California near Taylorsville: Geological Society of America, Abstracts with Programs, v. 46, no. 5, p. 25.
Christe, G., LaMaskin, T.A., and Schweickert, R.A., 2018, Implications of new detrital-zircon data for the depositional history, provenance, and paleogeography of Upper Triassic–Middle Jurassic rocks within the Northern Sierra terrane, California, USA, *in* Ingersoll, R.V., Lawton, T.F., and Graham, S.A., eds., Tectonics, Sedimentary Basins, and Provenance: A Celebration of William R. Dickinson's Career: Geological Society of America Special Paper 540, p. 297–318, https://doi.org/10.1130/2018.2540(13).
Colpron, M., and Nelson, J.L., 2009, A Paleozoic Northwest Passage: Incursion of Caledonian, Baltican and Siberian terranes into eastern Panthalassa, and the early evolution of the North American Cordillera, *in* Cawood, P.A., and Kröner, A., eds., Earth Accretionary Systems in Space and Time: Geological Society of London Special Publication 318, p. 273–307.
Davidson, J.P., Turner, S.P., and Plank, T., 2013, Dy/Dy*: Variations Arising from Mantle Sources and Petrogenetic Processes: Journal of Petrology, v. 54, no. 3, p. 525–537, https://doi.org/10.1093/petrology/egs076.
Day, H.W., and Bickford, M.E., 2004, Tectonic setting of the Jurassic Smartville and Slate Creek complexes, northern Sierra Nevada, California: Geological Society of America Bulletin, v. 116, p. 1515–1528, https://doi.org/10.1130/B25416.1.
Day, H.W., Moores, E.M., and Tuminas, A.C., 1985, Structure and tectonics of the northern Sierra Nevada: Geological Society of America Bulletin, v. 96, p. 436–450, https://doi.org/10.1130/0016-7606(1985)96<436:SATOTN>2.0.CO;2.
Dickinson, W.R., 2008, Accretionary Mesozoic–Cenozoic expansion of the Cordilleran continental margin in California and adjacent Oregon: Geosphere, v. 4, p. 329–353, https://doi.org/10.1130/GES00105.1.
Dickinson, W.R., and Gehrels, G.E., 2010, Insights into North American Paleogeography and Paleotectonics from U-Pb ages of detrital zircons in Mesozoic strata of the Colorado Plateau, USA: International Journal of Earth Sciences, v. 99, p. 1247–1265, https://doi.org/10.1007/s00531-009-0462-0.
Dilek, Y., Thy, P., and Moores, E.M., 1991, Episodic dike intrusions in the northwestern Sierra Nevada, California: Implications for multistage evolution of a Jurassic arc terrane: Geology, v. 19, p. 180–184, https://doi.org/10.1130/0091-7613(1991)019<0180:EDIITN>2.3.CO;2.
Ducea, M.N., 2001, The California arc: Thick granitic batholiths, eclogitic residues, lithospheric-scale thrusting, and magmatic flare-ups: GSA Today, v. 11, no. 11, p. 4–10, https://doi.org/10.1130/1052-5173(2001)011<0004:TCATGB>2.0.CO;2.
Dunne, G.C., and Suczek, C.A., 1991, Early Paleozoic eugeoclinal strata in the Kern Plateau pendants, southern Sierra Nevada, California, *in* Cooper, J.D., and Stevens, C.H., eds., Paleozoic Paleogeography of the Western United States: Los Angeles, California, Pacific Section, Society of Economic Paleontologists and Mineralogists (Book 67), p. 677–692.
Dunne, G.C., and Walker, J.D., 2004, Structure and evolution of the East Sierran thrust system, east central California: Tectonics, v. 23, no. 4, https://doi.org/10.1029/2002TC001478.
Edelman, S.H., and Sharp, W.D., 1989, Terranes, early faults, and pre-Late Jurassic amalgamation of the western Sierra Nevada metamorphic belt, California: Geological Society of America Bulletin, v. 101, p. 1420–1433, https://doi.org/10.1130/0016-7606(1989)101<1420:TEFAPL>2.3.CO;2.
Edelman, S.H., Day, H.W., Moores, E.M., Zigan, S., Murphy, T.P., and Hacker, B.R., 1989, Structure across a Mesozoic Ocean-Continent Suture Zone in the Northern Sierra Nevada, California: Geological Society of America Special Paper 224, 56 p., https://doi.org/10.1130/SPE224-p1.
Fiske, R.S., and Tobisch, O.T., 1978, Paleogeographic significance of volcanic rocks of the Ritter Range pendant, central Sierra Nevada, *in* Howell, D.G., and McDougall, K.A., eds., Mesozoic Paleogeography of the Western United States: Society of Economic Paleontologists and Mineralogists, Pacific Section, Pacific Coast Paleogeography Symposium 2, p. 209–222.
Fiske, R.S., and Tobisch, O.T., 1994, Middle Cretaceous ash-flow tuff and caldera-collapse deposit in the Minarets Caldera, east-central Sierra Nevada, California: Geological Society of America Bulletin, v. 106, no. 5, p. 582–593, https://doi.org/10.1130/0016-7606(1994)106<0582:MCAFTA>2.3.CO;2.

Gehrels, G., Valencia, V.A., and Ruiz, J., 2008, Enhanced precision, accuracy, efficiency, and spatial resolution of U-Pb ages by laser ablation–multicollector–inductively coupled plasma–mass spectrometry: Geochemistry, Geophysics, Geosystems, v. 9, no. 3, https://doi.org/10.1029/2007GC001805.

Gehrels, G.E., 2014, Detrital zircon U-Pb geochronology applied to tectonics: Annual Review of Earth and Planetary Sciences, v. 42, p. 127–149, https://doi.org/10.1146/annurev-earth-050212-124012.

Gehrels, G.E., and Pecha, M., 2014, Detrital zircon U-Pb geochronology and Hf isotope geochemistry of Paleozoic and Triassic passive margin strata of western North America: Geosphere, v. 10, p. 49–65, https://doi.org/10.1130/GES00889.1.

Graymer, R.W., and Jones, D.L., 1994, Tectonic implications of radiolarian cherts from the Placerville belt, Sierra Nevada Foothills, California: Nevadan-age continental growth by accretion of multiple terranes: Geological Society of America Bulletin, v. 106, no. 4, p. 531–540, https://doi.org/10.1130/0016-7606(1994)106<0531:TIORCF>2.3.CO;2.

Greene, D.C., and Schweickert, R.A., 1995, The Gem Lake shear zone: Cretaceous dextral transpression in the northern Ritter Range pendant, eastern Sierra Nevada, California: Tectonics, v. 14, p. 945–961, https://doi.org/10.1029/95TC01509.

Greene, D.C., Stevens, C.H., and Wise, J.M., 1997, The Laurel-Convict fault, eastern Sierra Nevada, California: A Permo-Triassic left-lateral fault, not a Cretaceous intrabatholithic break: Geological Society of America Bulletin, v. 109, no. 4, p. 483–488, https://doi.org/10.1130/0016-7606(1997)109<0483:TLCFES>2.3.CO;2.

Hamilton, W., 1969, Mesozoic California and the underflow of Pacific mantle: Geological Society of America Bulletin, v. 80, p. 2409–2430, https://doi.org/10.1130/0016-7606(1969)80[2409:MCATUO]2.0.CO;2.

Harwood, D.S., 1988, Tectonism and metamorphism in the Northern Sierra Terrane, northern California, *in* Ernst, W.G., ed., Metamorphism and Crustal Evolution of the Western United States (Rubey Volume VII): Englewood Cliffs, New Jersey, Prentice Hall, p. 764–788.

Harwood, D.S., 1992, Stratigraphy of Paleozoic and lower Mesozoic rocks in the northern Sierra terrane, California: U.S. Geological Survey Bulletin 1957, 78 p.

Herzig, C.T., and Sharp, W.D., 1992, The Sullivan Creek terrane: A composite Jurassic arc assemblage, western Sierra Nevada metamorphic belt, California: Geological Society of America Bulletin, v. 104, p. 1292–1300, https://doi.org/10.1130/0016-7606(1992)104<1292:TSCTAC>2.3.CO;2.

Jennings, C.W., with modifications by Gutierrez, C., Bryant, W., Saucedo, G., and Wills, C., 2010, Geologic map of California: California Geological Survey, Geologic Data Map Number 2, scale 1:750,000.

Kirsch, M., Paterson, S.R., Wobbe, F., Ardila, A.M.M., Clausen, B.L., and Alasino, P.H., 2016, Temporal histories of Cordilleran continental arcs: Testing models for magmatic episodicity: The American Mineralogist, v. 101, p. 2133–2154, https://doi.org/10.2138/am-2016-5718.

Kirkland, C.L., Smithies, R.H., Taylor, R.J.M., Evans, N., and McDonald, B., 2015, Zircon Th/U ratios in magmatic environs: Lithos, v. 212–215, p. 397–414, https://doi.org/10.1016/j.lithos.2014.11.021.

Kistler, R.W., 1993, Mesozoic intrabatholithic faulting, Sierra Nevada, California, *in* Dunne, G.C., and McDougall, K.A., eds., Mesozoic Paleogeography of the Western United States—II: Los Angeles, Pacific Section, Society of Economic Paleontologists and Mineralogists, Book 7, p. 247–261.

Kistler, R.W., and Ross, D.C., 1990, A strontium isotopic study of plutons and associated rocks of the southern Sierra Nevada vicinity, California: U.S. Geological Survey Bulletin 1920, 22 p.

Klemetti, E.W., Lackey, J.S., and Starnes, J., 2014, Magmatic lulls in the Sierra Nevada captured in zircon from rhyolite of the Mineral King pendant, California: Geosphere, v. 10, no. 1, p. 66–79, https://doi.org/10.1130/GES00920.1.

Laskowski, A.K., DeCelles, A.G., and Gehrels, G.E., 2013, Detrital zircon geochronology of Cordilleran retroarc foreland basin strata, western North America: Tectonics, v. 32, p. 1027–1048, https://doi.org/10.1002/tect.20065.

Ludwig, K.R., 2012, Isoplot/Ex 3.75: A Geochronological Toolkit for Microsoft Excel: Berkeley Geochronological Center Special Publication Number 5, 76 p.

Martin, M.W., and Clemens-Knott, D., 2015, Detrital-zircon record of the early Mesozoic southwestern Sierra Nevada arc preserved in Lower Cretaceous intra-arc and forearc deposits of central California, USA, *in* Anderson, T.H., Didenko, A.N., Johnson, C.L., Khanchuk, A.I., and MacDonald, J.H., Jr., eds., Late Jurassic Margin of Laurasia—A Record of Faulting Accommodating Plate Rotation: Geological Society of America Special Paper 513, p. 269–284, https://doi.org/10.1130/2015.2513(06).

Martin, M.W., and Walker, J.D., 1995, Stratigraphy and paleogeographic significance of metamorphic rocks in the Shadow Mountains, western Mojave Desert, California: Geological Society of America Bulletin, v. 107, p. 354–366, https://doi.org/10.1130/0016-7606(1995)107<0354:SAPSOM>2.3.CO;2.

Memeti, V., Gehrels, G.E., Paterson, S.R., Thompson, J.M., Mueller, R., and Pignotta, M., 2010, Evaluating the Mojave-Snow Lake fault hypothesis and origins of central Sierran metasedimentary pendant strata using detrital zircon provenance analyses: Lithosphere, v. 2, p. 341–360, https://doi.org/10.1130/L58.1.

Miller, J.S., Glazner, A.F., Walker, J.D., and Martin, M.W., 1995, Geochronologic and isotopic evidence for Triassic–Jurassic emplacement of the eugeoclinal allochthon in the Mojave Desert region, California: Geological Society of America Bulletin, v. 107, no. 12, p. 1441–1457, https://doi.org/10.1130/0016-7606(1995)107<1441:GAIEFT>2.3.CO;2.

Moores, E.M., 1970, Ultramafics and orogeny, with models for the U.S. Cordillera and the Tethys: Nature, v. 228, p. 837–842, https://doi.org/10.1038/228837a0.

Orme, D.A., and Surpless, K.D., 2019, The birth of a forearc: The basal Great Valley Group, California, USA: Geology, v. 47, p. 757–761, https://doi.org/10.1130/G46283.1.

Paterson, S.R., and Ducea, M.N., 2015, Arc magmatic tempos: Gathering the evidence: Elements, v. 11, no. 2, p. 91–98, https://doi.org/10.2113/gselements.11.2.91.

Paterson, S.R., and Memeti, V., 2014, Mesozoic volcanic rocks of the central Sierra Nevada arc, *in* Memeti, V., Paterson, S.R., and Putirka, K.D., eds., Formation of the Sierra Nevada Batholith: Magmatic and Tectonic Processes and Their Tempos: Geological Society of America Field Guide 34, p. 75–85.

Paterson, S.R., Tobisch, O.T., and Radioif, J.K., 1987, Post-Nevadan deformation along the Bear Mountains fault zone: Implications for the Foothills terrane, central Sierra Nevada, California: Geology, v. 15, p. 513–516, https://doi.org/10.1130/0091-7613(1987)15<513:PDATBM>2.0.CO;2.

Paterson, S.R., Tobisch, O.T., and Bhattacharyya, T., 1989, Regional, structural and strain analyses of terranes in the Western Metamorphic Belt, Central Sierra Nevada, California: Journal of Structural Geology, v. 11, p. 255–273, https://doi.org/10.1016/0191-8141(89)90066-7.

Paterson, S.R., Clausen, B.L., Memeti, V., and Schwartz, J.J., 2017, Arc magmatism, tectonism, and tempos in Mesozoic arc crustal sections of the Peninsular and Transverse Ranges, southern California, USA, *in* Kraatz, B., Lackey, J.S., and Fryxell, J.E., eds., Field Excursions in Southern California: Field Guides to the 2016 GSA Cordilleran Section Meeting: Geological Society of America Field Guide 45, p. 81–186, https://doi.org/10.1130/2017.0045(04).

Paterson, S.R., Attia, S., Ardill, K.E., and Wesley, A.J., 2019, Time series perspective of evolving Jurassic arc behavior in the central Sierra Nevada arc: Geological Society of America Abstracts with Programs, v. 51, no. 5, https://doi.org/10.1130/abs/2019AM-339616.

Powerman, V., Hanson, R., Nosova, A., Girty, G.H., Hourigan, J., and Tretiakov, A., 2020, Nature and timing of Late Devonian–early Mississippian island-arc magmatism in the Northern Sierra terrane and implications for regional Paleozoic plate tectonics: Geosphere, v. 16, no. 1, p. 258–280, https://doi.org/10.1130/GES02105.1.

Proffett, J.M., and Dilles, J.H., 2008, Lower Mesozoic sedimentary and volcanic rocks of the Yerington region, Nevada, and their regional context, *in* Wright, J.E., and Shervais, J.W., eds., Ophiolites, Arcs, and Batholiths: A Tribute to Cliff Hopson: Geological Society of America Special Paper 438, p. 251–288, https://doi.org/10.1130/2008.2438(09).

Rains, J.L., Marsaglia, K.M., and Dunne, G.C., 2012, Stratigraphic record of subduction initiation in the Permian metasedimentary succession of the El Paso Mountains, California: Lithosphere, v. 4, no. 6, p. 533–552, https://doi.org/10.1130/L165.1.

Riggs, N.R., Reynolds, S.J., Lindner, P.J., Howell, E.R., Barth, A.P., Parker, W.G., and Walker, J.D., 2013, The Early Mesozoic Cordilleran arc and Late Triassic paleotopography: The detrital record in Upper Triassic sedimentary successions on and off the Colorado Plateau: Geosphere, v. 9, no. 3, p. 602–613, https://doi.org/10.1130/GES00860.1.

Riggs, N.R., Oberling, Z.A., Howell, E.R., Parker, W.G., Barth, A.P., Cecil, M.R., and Martz, J.W., 2016, Sources of volcanic detritus in the basal Chinle Formation, southwestern Laurentia, and implications for the Early Mesozoic magmatic arc: Geosphere, v. 12, no. 2, p. 439–463, https://doi.org/10.1130/GES01238.1.

Russell, L.R., and Cebull, S.E., 1977, Structural-metamorphic chronology in a roof pendant near Oakhurst, California: Implications for the tectonics of the western Sierra Nevada: Geological Society of America Bulletin, v. 88, p. 1530–1534, https://doi.org/10.1130/0016-7606(1977)88<1530:SCIARP>2.0.CO;2.

Saleeby, J., 1979, Kaweah serpentinite mélange, southwest Sierra Nevada foothills, California: Geological Society of America Bulletin, v. 90, no. 1, p. 29–46, https://doi.org/10.1130/0016-7606(1979)90<29:KSMSSN>2.0.CO;2.

Saleeby, J., 2007, Western extent of the Sierra Nevada batholith in the Great Valley Basement: Eos (Transactions, American Geophysical Union), v. 88, no. 52, F2186.

Saleeby, J., 2011, Geochemical mapping of the Kings-Kaweah ophiolite belt, California—Evidence for progressive mélange formation in a large offset transform-subduction initiation environment, *in* Wakabayashi, J., and Dilek, Y., eds., Mélanges: Processes of Formation and Societal Significance: Geological Society of America Special Paper 480, p. 31–73, https://doi.org/10.1130/2011.2480(02).

Saleeby, J., and Dunne, G., 2015, Temporal and tectonic relations of early Mesozoic arc magmatism, southern Sierra Nevada, California, *in* Anderson, T.H., Didenko, A.N., Johnson, C.L., Khanchuk, A.I., and MacDonald, J.H., Jr., eds., Late Jurassic Margin of Laurasia—A Record of Faulting Accommodating Plate Rotation: Geological Society of America Special Paper 513, p. 223–268, https://doi.org/10.1130/2015.2513(05).

Saleeby, J.B., 1982, Polygenetic ophiolite belt of the California Sierra Nevada, geochronological and tectonostratigraphic development: Journal of Geophysical Research, v. 87, p. 1803–1824, https://doi.org/10.1029/JB087iB03p01803.

Saleeby, J.B., 1990, Geochronological and tectonostratigraphic framework of Sierran-Klamath ophiolitic assemblages, *in* Harwood, D.S., and Miller, M.M., eds., Paleozoic and Early Mesozoic Paleogeographic Relations; Sierra Nevada, Klamath Mountains, and Related Terranes: Geological Society of America Special Paper 255, p. 93–114, https://doi.org/10.1130/SPE255-p93.

Saleeby, J.B., and Busby, C., 1993, Paleogeographic and tectonic setting of axial and western metamorphic framework rocks of the southern Sierra Nevada, California, *in* Dunne, G., and McDougall, K., eds., Mesozoic Paleogeography of the Western United States—II: Los Angeles, California: Pacific Section, Society of Economic Paleontologists and Mineralogists Book 71, p. 197–225.

Saleeby, J.B., and Busby-Spera, C., 1986, Fieldtrip guide to the metamorphic framework rocks of the Lake Isabella area, southern Sierra Nevada, California, *in* Dunne, G.C., ed., Mesozoic and Cenozoic Structural Evolution of Selected Areas, East-Central California: Los Angeles, California: Cordilleran Section, Geological Society of America, Guidebook Volume, p. 81–94.

Saleeby, J.B., Shaw, H.F., Niemeyer, S., Edelman, S.H., and Moores, E.M., 1989, U/Pb, Sm/Nd and Rb/Sr geochronological and isotopic study of northern Sierra Nevada ophiolitic assemblages, California: Contributions to Mineralogy and Petrology, v. 102, p. 205–220, https://doi.org/10.1007/BF00375341.

Saleeby, J.B., Kistler, R.W., Longiaru, S., Moore, J.G., and Nokleberg, W.J., 1990, Middle Cretaceous silicic metavolcanic rocks in the Kings Canyon area, central Sierra Nevada, California, *in* Anderson, J.L, ed., The Nature and Origin of Cordilleran Magmatism: Geological Society of America Memoir 174, p. 251–271, https://doi.org/10.1130/MEM174-p251.

Schweickert, R.A., 2015 Jurassic evolution of the Western Sierra Nevada metamorphic province, *in* Anderson, T.H., Didenko, A.N., Johnson, C.L., Khanchuk, A.I., and MacDonald, J.H., Jr., eds., Late Jurassic Margin of Laurasia—A Record of Faulting Accommodating Plate Rotation: Geological Society of America Special Paper 513, p. 299–358, https://doi.org/10.1130/2015.2513(08).

Schweickert, R.A., and Cowan, D.S., 1975, Early Mesozoic tectonic evolution of the western Sierra Nevada, California: Geological Society of America Bulletin, v. 86, p. 1329–1336, https://doi.org/10.1130/0016-7606(1975)86<1329:EMTEOT>2.0.CO;2.

Schweickert, R.A., and Lahren, M.M., 1990, Speculative reconstruction of a major Early Cretaceous(?) dextral fault zone in the Sierra Nevada: Implications for Paleozoic and Mesozoic orogenesis in the western United States: Tectonics, v. 9, p. 1609–1629, https://doi.org/10.1029/TC009i006p01609.

Schweickert, R.A., and Lahren, M.M., 1993, Tectonics of the east-central Sierra Nevada-Saddleback Lake and northern Ritter Range pendants, *in* Lahren, M.M., Trexler, J.H., and Spinoza, C., eds., Crustal Evolution of the Great Basin and the Sierra Nevada: Reno, Nevada, Geological Society of America Field Trip Guidebook, May 1993, Department of Geological Sciences, University of Nevada, p. 313–352.

Schweickert, R.A., and Lahren, M.M., 2006, Geologic evolution of Saddlebag Lake pendant, eastern Sierra Nevada, California: Tectonic implications, *in* Girty, G., and Cooper, J.D., eds., Using Stratigraphy, Sedimentology, and Geochemistry to Unravel the Geologic History of the Southwestern Cordillera: Fullerton, California, Pacific Section, Society for Sedimentary Geology (SEPM), Book 101, p. 27–56.

Schweickert, R.A., Saleeby, J.B., Tobisch, O.T., and Wright, W.H., 1977, Paleotectonic and paleogeographic significance of the Calaveras complex, western Sierra Nevada, California, *in* Stewart, J.H., and Stevens, C.H., eds., Paleozoic Paleogeography of the Western United States: Society of Economic Paleontologists and Mineralogists, Pacific Section, p. 381–394.

Schweickert, R.A., Armstrong, R.L., and Harakal, J.E., 1980, Lawsonite blueschist in the northern Sierra Nevada, California: Geology, v. 8, p. 27–31, https://doi.org/10.1130/0091-7613(1980)8<27:LBITNS>2.0.CO;2.

Schweickert, R.A., Bogen, N.L., Girty, G.H., Hanson, R.E., and Merguerian, C., 1984, Timing and structural expression of the Nevadan orogeny, Sierra Nevada, California: Geological Society of America Bulletin, v. 95, no. 8, p. 967–969, https://doi.org/10.1130/0016-7606(1984)95<967:TASEOT>2.0.CO;2.

Schweickert, R.A., Merguerian, C., and Bogen, N.L., 1988, Deformational and metamorphic history of Paleozoic and Mesozoic basement terranes in the western Sierra Nevada metamorphic belt, *in* Ernst, W.G., ed., Metamorphism and Crustal Evolution of the Western United States, Rubey Volume VII: Englewood Cliffs, New Jersey, Prentice-Hall, Inc., p. 789–820.

Sharp, W.D., Tobisch, O.T., and Renne, P.R., 2000, Development of Cretaceous transpressional cleavage synchronous with batholith emplacement, central Sierra Nevada, California: Geological Society of America Bulletin, v. 112, p. 1059–1066, https://doi.org/10.1130/0016-7606(2000)112<1059:DOCTCS>2.0.CO;2.

Sigloch, K., and Mihalyunk, M.G., 2017, Mantle and geological evidence for a Late Jurassic–Cretaceous suture spanning North America: Geological Society of America Bulletin, v. 129, no. 11–12, p. 1489–1520, https://doi.org/10.1130/B31529.1.

Smart, C.M., and Wakabayashi, J., 2009, Hot and deep: Rock record of subduction initiation and exhumation of high-temperature, high-pressure metamorphic rocks, Feather River ultramafic belt, California: Lithos, v. 113, p. 292–305, https://doi.org/10.1016/j.lithos.2009.06.012.

Snow, C., 2007, Petrotectonic evolution and melt modeling of the Peñon Blanco arc, central Sierra Nevada foothills, California: Geological Society of America Bulletin, v. 119, p. 1014–1024, https://doi.org/10.1130/B25972.1.

Snow, C., and Ernst, W.G., 2008, Detrital zircon constraints on sediment distribution and provenance of the Mariposa Formation, central Sierra Nevada foothills, California, *in* Wright, J.E., and Shervais, J.W., eds., Ophiolites, Arcs, and Batholiths: A Tribute to Cliff Hopson: Geological Society of America Special Paper 438, p. 311–330, https://doi.org/10.1130/2008.2438(11).

Snow, C., and Scherer, H.H., 2006, Terranes of the western Sierra Nevada foothills: A critical review: International Geology Review, v. 48, p. 46–62, https://doi.org/10.2747/0020-6814.48.1.46.

Sorensen, S.S., Dunne, G.C., Hanson, R.B., Barton, M.D., Becker, J., Tobisch, O.T., and Fiske, R.S., 1998, From Jurassic shores to Cretaceous plutons: Geochemical evidence for paleoalteration environments of metavolcanic rocks, eastern California: Geological Society of America Bulletin, v. 110, no. 3, p. 326–343, https://doi.org/10.1130/0016-7606(1998)110<0326:FJSTCP>2.3.CO;2.

Spurlin, M.S., Gehrels, G.E., and Harwood, D.S., 2000, Detrital zircon geochronology of upper Paleozoic and lower Mesozoic strata of the northern Sierra terrane, northeastern California, *in* Soreghan, M.J., and Gehrels, G.E., eds., Paleozoic and Triassic Paleogeography and Tectonics of Western Nevada and Northern California: Geological Society of America Special Paper 347, p. 89–98, https://doi.org/10.1130/0-8137-2347-7.89.

Stevens, C.H., and Greene, D.C., 1999, Stratigraphy, depositional history, and tectonic evolution of Paleozoic continental-margin rocks in roof pendants of the eastern Sierra Nevada, California: Geological Society of America Bulletin, v. 111, p. 919–933, https://doi.org/10.1130/0016-7606(1999)111<0919:SDHATE>2.3.CO;2.

Stevens, C.H., Stone, P., and Miller, J.S., 2005, A new reconstruction of the Paleozoic continental margin of southwest North America: Implications for the nature and timing of continental truncation and the possible role of the Mojave-Sonora megashear, *in* Anderson, T.H., Nourse, J.A., McKee, J.W., and Steiner, M.B., eds., The Mojave-Sonora Megashear Hypothesis: Development, Assessment, and Alternatives: Geological Society of America Special Paper 393, p. 597–618.

Stone, P., and Stevens, C.H., 1988, An angular unconformity in the Permian section of east-central California: Geological Society of America Bulletin, v. 100, p. 547–551, https://doi.org/10.1130/0016-7606(1988)100<0547:AAUITP>2.3.CO;2.

Stone, P., Barth, A.P., Wooden, J.L., Fohey-Breting, N.K., Vazquez, J.A., and Priest, S.S., 2013, Geochronologic and geochemical data from Mesozoic rocks in the Black Mountain area northeast of Victorville, San Bernardino County, California: U.S. Geological Survey Open-File Report 2013-1146, 31 p., https://doi.org/10.3133/ofr20131146.

Sundell, K.E., Saylor, J.E., and Pecha, M., 2019, Sediment provenance and recycling of detrital zircons from Cenozoic Altiplano strata in southern Peru and implications for the crustal evolution of west-central South America, *in* Horton, K.B., and Folguera, A., eds., Andean Tectonics: Elsevier, p. 363–397, https://doi.org/10.1016/B978-0-12-816009-1.00014-9.

Surpless, K.D., Clemens-Knott, D., Barth, A.P., and Gevedon, M., 2019, A survey of Sierra Nevada magmatism using Great Valley detrital zircon trace-element geochemistry: View from the forearc: Lithosphere, v. 11, no. 5, p. 603–619, https://doi.org/10.1130/L1059.1.

Thomas, W.A., 2011, Detrital-zircon geochronology and sedimentary provenance: Lithosphere, v. 3, p. 304–308, https://doi.org/10.1130/RF.L001.1.

Tobisch, O.T., Fiske, R.S., Sacks, S., and Taniguchi, D., 1977, Strain in metamorphosed volcaniclastic rocks and its bearing on the evolution of orogenic belts: Geological Society of America Bulletin, v. 88, p. 23–40, https://doi.org/10.1130/0016-7606(1977)88<23:SIMVRA>2.0.CO;2.

Tobisch, O.T., Paterson, S.R., Saleeby, J.B., and Geary, E.E., 1989, Nature and timing of deformation in the Foothills terrane, central Sierra Nevada, California: Its bearing on orogenesis: Geological Society of America Bulletin, v. 101, p. 401–413, https://doi.org/10.1130/0016-7606(1989)101<0401:NATODI>2.3.CO;2.

Tobisch, O.T., Saleeby, J.B., Renne, P.R., McNulty, B., and Tong, W., 1995, Variations in deformation fields during development of a large-volume magmatic arc, central Sierra Nevada, California: Geological Society of America Bulletin, v. 107, p. 148–166, https://doi.org/10.1130/0016-7606(1995)107<0148:VIDFDD>2.3.CO;2.

Tobisch, O.T., Fiske, R.S., Saleeby, J.B., Holt, E., and Sorensen, S.S., 2000, Steep tilting of metavolcanic rocks by multiple mechanisms, central Sierra Nevada, California: Geological Society of America Bulletin, v. 112, p. 1043–1058, https://doi.org/10.1130/0016-7606(2000)112<1043:STOMRB>2.0.CO;2.